iScience

CellPress
OPEN ACCESS

Article

Kidney fibrosis molecular mechanisms Spp1 influences fibroblast activity through transforming growth factor beta smad signaling

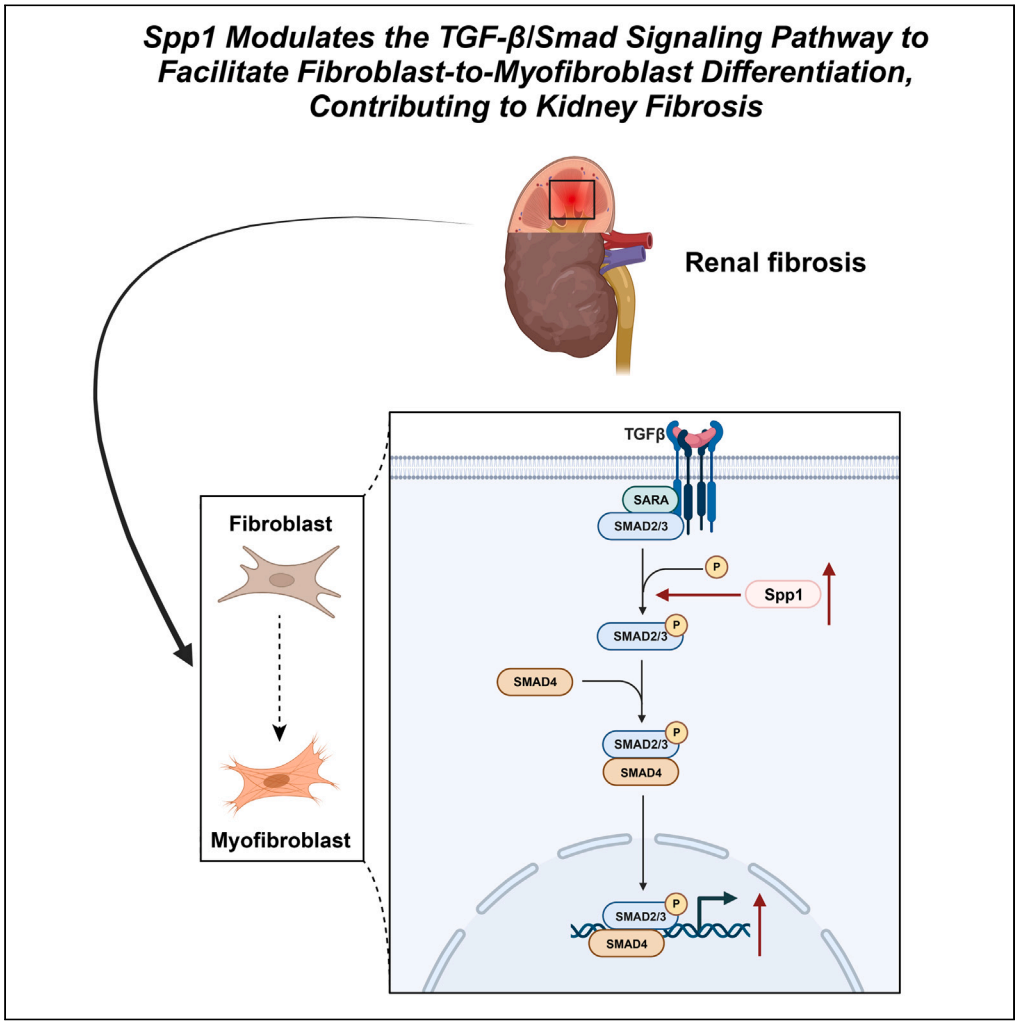

Hao Ding, Zidu Xu, Ying Lu, Qi Yuan, Jianzhong Li, Qi Sun

lijianzhong1511@suda.edu.cn (J.L.)
sunqi@njmu.edu.cn (Q.S.)

Highlights

Unveils Spp1's key role in kidney fibrosis via the TGF-β/Smad pathway

Uses single-cell sequencing to deeply analyze cellular heterogeneity in fibrosis

Identifies Spp1 as a potential therapeutic target for kidney fibrosis

Validates Spp1's effect on fibroblast behavior by *in vivo* and *in vitro* experiments

Ding et al., iScience 27, 109839
September 20, 2024
https://doi.org/10.1016/j.isci.2024.109839

iScience

CellPress
OPEN ACCESS

Article

Kidney fibrosis molecular mechanisms Spp1 influences fibroblast activity through transforming growth factor beta smad signaling

Hao Ding,[1,7] Zidu Xu,[2,7] Ying Lu,[3] Qi Yuan,[4] Jianzhong Li,[5,*] and Qi Sun[6,8,*]

SUMMARY

Kidney fibrosis marks a critical phase in chronic kidney disease with its molecular intricacies yet to be fully understood. This study's deep dive into single-cell sequencing data of renal tissue during fibrosis pinpoints the pivotal role of fibroblasts and myofibroblasts in the fibrotic transformation. Through identifying distinct cell populations and conducting transcriptomic analysis, Spp1 emerged as a key gene associated with renal fibrosis. The study's experimental findings further confirm Spp1's vital function in promoting fibroblast to myofibroblast differentiation via the TGF-β/Smad signaling pathway, underscoring its contribution to fibrosis progression. The suppression of Spp1 expression notably hindered this differentiation process, spotlighting Spp1 as a promising therapeutic target for halting renal fibrosis. This condensed summary encapsulates the essence and findings of the original research within the specified word limit.

INTRODUCTION

Renal fibrosis is a late-stage pathological manifestation of chronic kidney disease, characterized predominantly by tubular atrophy, interstitial fibrosis, and glomerulosclerosis.[1] The emergence of renal damage is not solely attributed to intrinsic kidney factors but is intricately connected to multiple elements, including inflammation, oxidative stress, and the excessive activation of growth factors.[2] Prolonged persistence of renal fibrosis can result in the enduring degradation of kidney function, a key driver of the development of end-stage renal disease.[3] Managing fibrosis poses formidable challenges due to the intricate engagement of numerous intricate cellular and molecular mechanisms in its progression.[4] Current therapeutic approaches typically focus on slowing and advancing fibrosis rather than achieving complete reversal.[5] Therefore, the presence of renal fibrosis often signifies an unfavorable prognosis, frequently necessitating long-term reliance on dialysis or kidney transplantation.[6] Addressing this formidable enigma necessitates extensive research endeavors and the formulation of innovative treatment strategies, both of which have emerged as critical priorities.[7]

The conversion of fibroblasts into myofibroblasts constitutes a pivotal occurrence in the development of renal fibrosis.[8] During this transformation, fibroblasts undergo a profound alteration, shedding their original characteristics and adopting the attributes of myofibroblasts. Consequently, they actively contribute to the progression of fibrosis.[9] Genes characteristic of fibroblasts, including α-SMA, vimentin, and collagen I, exhibit heightened expression, signifying the commencement of the fibroblast-to-myofibroblast transition process. This process serves as a crucial signal in the advancement of fibrosis.[10] The increased expression of these genes in renal fibrosis is highly correlated with the gradual deterioration of renal function.[11] Consequently, targeting the regulation of these marker genes offers innovative strategies and avenues for therapeutic intervention in renal fibrosis.[12]

Leveraging state-of-the-art single-cell data analysis, this investigation embarks on a comprehensive examination of the specific genes intricately involved in the intricate process of renal fibrosis.[13] The findings thrust Spp1 into the spotlight as a pivotal gene exhibiting a robust connection with fibroblast behavior.[14] Since fibroblasts assume the mantle of primary effector cells in renal fibrosis, shifts in Spp1 expression, emerge as a direct gauge of fibrosis progression.[15] Subsequent analysis delves into the possibility that Spp1 wields its influence on renal fibrosis by orchestrating the regulation of the TGF-β/Smad signaling pathway.[16] Despite the undeniable significance of this signaling pathway in fibrosis, the precise molecular mechanisms governing its control by Spp1 remain uncertain.[17] To attain a more profound grasp of Spp1's role in renal fibrosis, additional experimental investigations become imperative to unravel its intricate interplay with the TGF-β/Smad

[1]Center for Kidney Disease, Second Affiliated Hospital of Nanjing Medical University, Nanjing 210000, P.R. China
[2]Emergency Medicine Center, Second Affiliated Hospital of Nanjing Medical University, Nanjing 210000, P.R. China
[3]Department of Group Healthcare, First Affiliated Hospital of Nanjing Medical University, Nanjing 210000, P.R. China
[4]Department of Nephrology, The Affiliated Suzhou Hospital of Nanjing Medical University, Nanjing 215000, P.R. China
[5]Department of Nephrology, The First Affiliated Hospital of Soochow University, Suzhou 215006, P.R. China
[6]Nanjing Medical University, Nanjing 211166, P.R. China
[7]These authors contributed equally
[8]Lead contact
*Correspondence: lijianzhong1511@suda.edu.cn (J.L.), sunqi@njmu.edu.cn (Q.S.)
https://doi.org/10.1016/j.isci.2024.109839

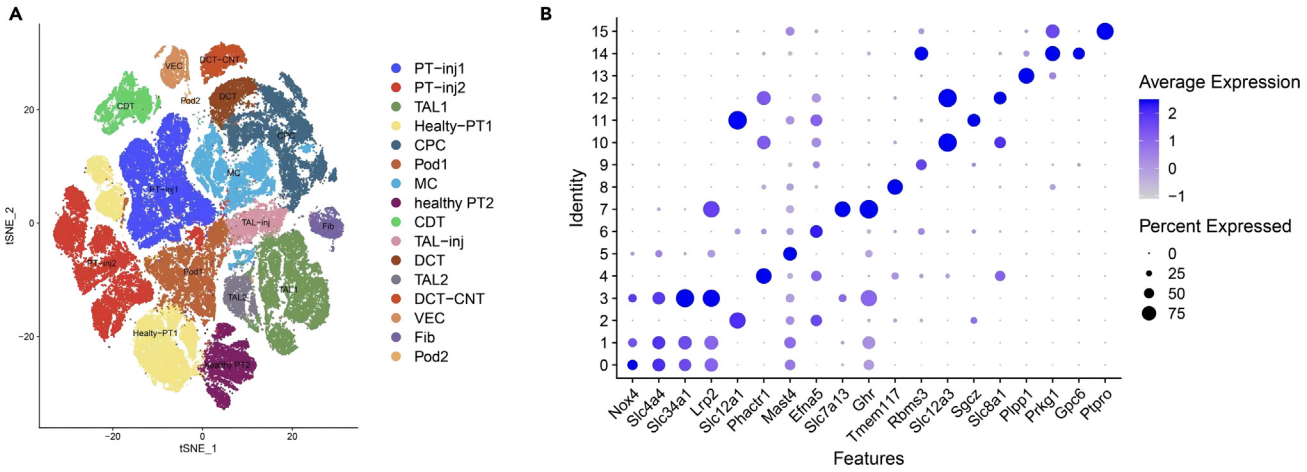

Figure 1. Analysis of Cell Cluster Annotation

(A) Annotation of 16 cell clusters.

(B) Bubble plot showing the expression of marker genes in each cell cluster.

signaling pathway.[18] This groundbreaking revelation promises to pave the way for the identification of novel therapeutic targets and the pioneering of innovative treatment strategies for renal fibrosis.[19]

Considering the pivotal role of Spp1 in various diseases, the aim of this study is to deeply investigate the molecular mechanisms of Spp1 in renal fibrosis, elucidating its involvement in regulating fibroblast behavior and its relationship with the TGF-β/Smad signaling pathway during the process of renal fibrosis. By gaining a thorough understanding of this process, we hope to provide novel targets for the treatment of renal fibrosis and offer theoretical support for clinical therapy. Furthermore, this study will contribute to enhancing our overall comprehension of fibrotic mechanisms, laying a solid foundation for future research on fibrosis treatment.

RESULTS

Single-cell RNA sequencing analysis reveals distinct cell clusters and their expression patterns in mouse kidney following ischemia-reperfusion injury

We obtained the single-cell transcriptomic dataset GSE139107 related to acute kidney injury from the Gene Expression Omnibus (GEO). The data were integrated using the Seurat package, and we examined the gene counts (nFeature_RNA), mRNA molecule counts (nCount_RNA), and percentage of mitochondrial genes (percent.mt) for all cells in the scRNA-seq dataset. The analysis revealed that the majority of cells had nFeature_RNA <1500, nCount_RNA <10000, and percent.mt < 1.5% (Figure S1A).

Low-quality cells were removed based on the criteria of nFeature_RNA >300, 300 < nCount_RNA <5000, and percent.mt < 3%. The correlation analysis of sequencing depth revealed a coefficient of r = 0.12 between nCount_RNA and percent.mt and a coefficient of r = 0.73 between nCount_RNA and nFeature_RNA (Figure S1B). These results indicate that the filtered cell data exhibits good quality and can be used for subsequent analysis.

The filtered cells were further analyzed by applying the "LogNormalize" function for data standardization. Subsequently, the top 2000 genes with high variability were selected for downstream analysis based on their variance (Figure S1C). The dimensionality reduction technique, PCA (Principal Component Analysis), was then employed on these selected genes, resulting in 40 principal components (PCs). The first 20 PCs were chosen for subsequent t-SNE clustering and cell annotation (Figure S1D). The PCA analysis results for each cell in every sample are presented in Figure S1E. The characteristic genes of the first two principal components are displayed in Figure S1F, and the expression heatmap of these genes is shown in Figure S1G.

The above results indicate that the PCA principal component analysis result is relatively reliable and could be used for subsequent cell clustering.

After the TSNE clustering analysis, we clustered all the cells into 16 clusters (Figure S2A). The distribution of each cell cluster in each sample is shown in Figure S2B.

Next, the 16 cell populations were annotated based on known cell lineage-specific marker genes from the literature and using the online database CellMarker (Figure 1A). The annotation results included the following cell types: PT-inj1 (injured proximal tubule type 1), PT-inj2 (injured proximal tubule type 2), TAL1 (ascending thin limb of Henle's loop type 1), Healthy-PT1 (healthy proximal tubule type 1), CPC (collecting duct principal cells), Pod1 (podocyte type 1), MC (mesangial cells), Healthy-PT2 (healthy proximal tubule type 2), CDT (collecting duct transient cells), TAL-inj (injured ascending thin limb of Henle's loop), DCT (distal convoluted tubule), TAL2 (ascending thin limb of Henle's loop type 2), DCT-CNT (distal convoluted tubule and connecting tubule), VEC (vascular endothelial cells), Fib (fibroblasts), and Pod2

(podocyte type 2). Figures 1B and 2 showed the expression patterns of marker genes in various cell clusters. Through the above analysis, we have successfully annotated 16 cell types in the IRI single-cell sequencing dataset.

Characterization and evolutionary dynamics of fibroblast subpopulations in renal fibrosis

Fibroblasts play a critical role in kidney fibrosis. Their abnormal activation and proliferation lead to collagen deposition and fibrotic tissue formation.[20,21] Research shows that fibroblasts exhibit heterogeneity and may exist in multiple subpopulations, each with different functions during the process of fibrosis.[22] Therefore, we performed sub-clustering of fibroblasts to uncover the regulatory mechanisms of renal fibrosis.

First, all cells related to Fib cell clusters were extracted from the entire experimental dataset. Then, these cells underwent preprocessing steps, such as data standardization, feature selection for variability, and data scaling. Next, principal component analysis and clustering algorithms were used to divide the cells into different subgroups based on their gene expression similarities. Finally, t-distributed stochastic neighbor embedding (t-SNE) was employed to cluster all cells into nine subclusters (Figure 3A).

We annotated the cells based on existing literature and combined them with the online website CellMarker (Figure 3C). Cluster 0 is marked by the genes Dapk2 (Figures 3B and 3D) and annotated as "fibroblast type 1" (fib1); Cluster 1 is marked by the genes Sdc4 and Spp1 (Figures 3B and 3D–3F) and annotated as "fibroblast type 2" (fib2); Both cluster 2 and cluster 7 are marked by the genes Col1a1 and Col1a2 (Figures 3L and 3M) and therefore respectively annotated as "muscle fibroblast type 1" (mFib1) and "muscle fibroblast type 3" (mFib3); Cluster 3 is marked by the genes Kcnd2 (Figure 3G) and Bmpr1b (Figure 3H) and annotated as "fibroblast type 3" (fib3). The cluster 4 marker gene is Ank3 (Figures 3B and 3I), annotated as "cortical cells." Cluster 5 is marked by the gene Myh11 (Figures 3B and 3J) and annotated as "smooth muscle cells"; Cluster 6 is marked by the gene GPX3 (Figures 3B and 3K) and annotated as "myofibroblast type 2" (mFib2); Cluster 8 is marked by the gene Vcan (Figures 3B and 3N) and annotated as "fibroblast type 5" (fib5).

The above results indicate that the 9 cell clusters obtained through sub-clustering include different types of fibroblasts, smooth muscle cells, and cortical cells. The expression of marker genes and functional differences in these cell clusters reflect the heterogeneity of fibroblasts in the renal fibrosis process.

To gain a deeper understanding of the functional characteristics of these nine cell clusters, we performed gene ontology (GO) and KEGG pathway enrichment analysis on the marker genes of each cluster. Each cluster exhibited specific functional traits, such as cell adhesion, signal transduction, glomerular development, and muscular system development, revealing their significant roles in cell morphology, migration, signal transduction, and extracellular matrix formation. In cluster 0, we observed that its marker genes are primarily involved in biological processes such as cell-matrix adhesion, Ras protein signaling, and glomerular development, as well as enrichment in cellular components such as cell leading edge, leading edge membrane, and plasma membrane rafts. Additionally, these genes play roles in key signaling pathways, including focal adhesion, the cGMP-PKG signaling pathway, and ECM-receptor interaction (Figure 4A). These enrichment results suggest that cells in cluster 0 may play essential roles in cell adhesion, signal transduction, renal glomerular development, and the formation and function of the extracellular matrix.

In cluster 1, the marker genes are primarily enriched in biological processes such as cell-matrix adhesion, fibroblast migration, and the formation and functionality of the extracellular matrix. Additionally, these genes also exhibit involvement in key pathways, including ECM-receptor interaction, focal adhesion, and the PI3K-Akt signaling pathway (Figure 4B). These enrichment results revealed that cells in cluster 1 may play a key role in regulating cell adhesion, fibroblast migration, and the formation and function of extracellular matrix.

In cluster 2, the marker genes are primarily enriched in biological processes such as the organization of the cell cytoskeleton, the organization of the extracellular matrix, and the organization of collagen fibers. Additionally, these genes also exhibit involvement in key pathways including protein digestion and absorption, ECM-receptor interaction, and the PI3K-Akt signaling pathway (Figure 4C). These enrichment results suggest that cells in cluster 2 play essential roles in processes such as the organization of the cytoskeleton, the organization of the extracellular matrix, and the organization of collagen fibers.

In cluster 3, the marker genes are primarily involved in processes related to regulating cell component movement and cell migration, as well as being enriched in the Wnt signaling pathway. Additionally, these genes are expressed in cell components such as collagen-containing extracellular matrix, collagen trimers, and interstitial matrix. These genes are also closely associated with molecular functions such as beta-catenin binding and SMAD binding. Moreover, these genes play a role in biological pathways such as Gap junction and protein digestion and absorption (Figure 4D). These enrichment results indicate that cells in cluster 3 may play a critical role in regulating processes such as cell migration, the Wnt signaling pathway, and the organization of the extracellular matrix.

In cluster 4, the marker genes are primarily enriched in critical biological processes such as kidney development, the Wnt signaling pathway, and mesenchymal development. They also participate in the formation of cellular structures like the cell cortex and adherens junctions. Additionally, these genes show involvement in important biological pathways including resistance to EGFR tyrosine kinase inhibitors, the PI3K-Akt signaling pathway, and the MAPK signaling pathway (Figure 4E). These enrichment results reveal the potentially important roles of these cells in the development and signaling of the renal system.

For cluster 5, its marker genes are primarily enriched in critical biological processes such as muscle system process, cell development, and migration. They also form muscle cell structures, such as muscle fibers and myotubes. In addition, these genes also exhibit critical biological pathways such as vascular smooth muscle contraction, the cGMP-PKG signaling pathway, and the Apelin signaling pathway (Figure 4F). These enrichment results suggest that these cells may play an essential role in the development and function of the muscular system.

For cluster 6, we note that its marker genes are mainly enriched in biological processes such as the positive regulation of cellular protrusion organization, the integrin-mediated signaling pathway, and regulation of cell morphogenesis involved in differentiation. At the same time,

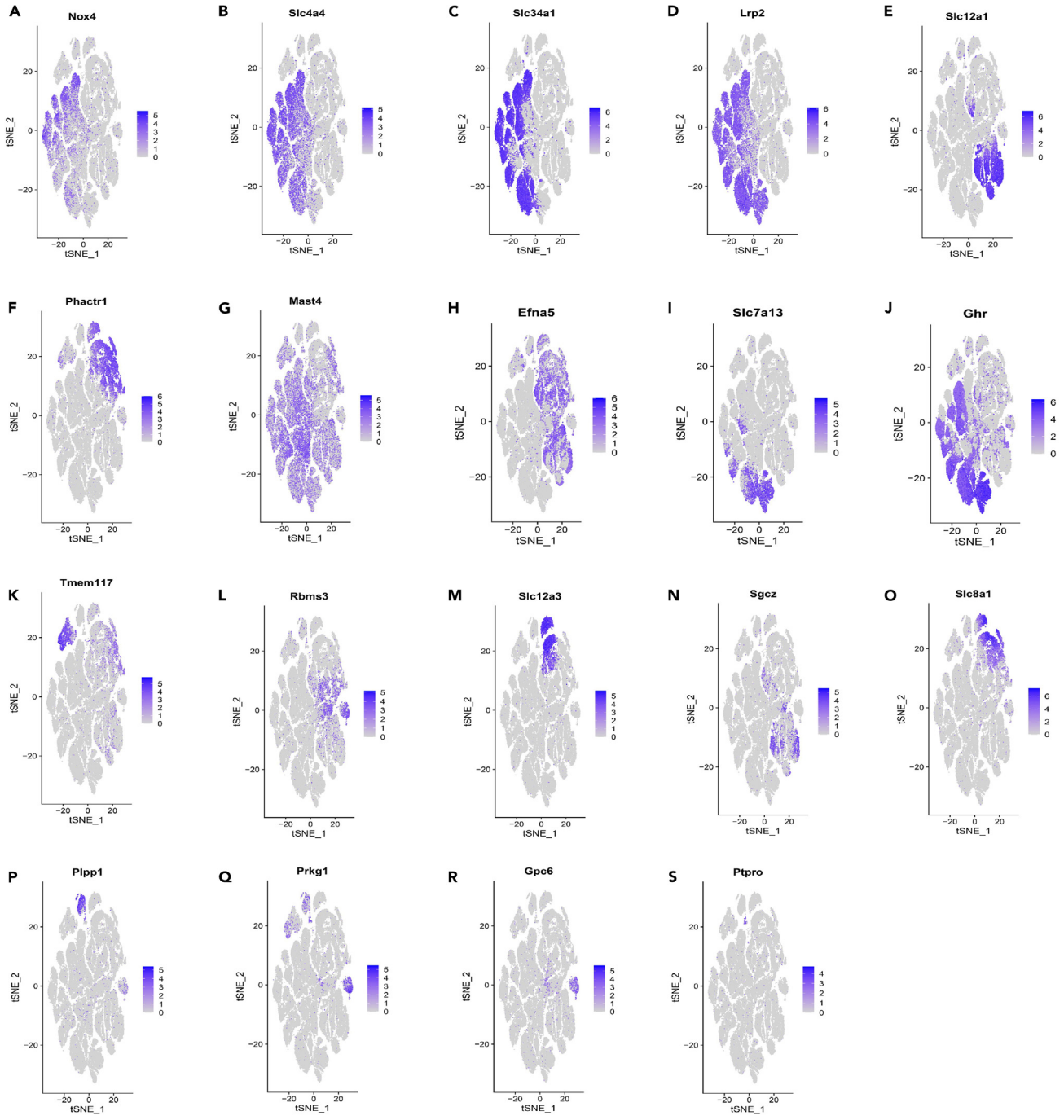

Figure 2. Analysis of Marker Gene Expression in Each Cell Cluster

(A–S) Cluster scatterplots showing the expression of marker genes in each cell cluster, with a darker blue color indicating higher average expression levels.

these genes also play a role in the composition of the synaptic membrane, especially in the intrinsic components of the glutamatergic synapses and synaptic membranes (Figure 4G). These enrichment results suggest that cells in cluster 6 may play essential roles in regulating cell morphology, signal transduction, and synaptic function.

For cluster 7, its signature genes are mainly enriched in biological processes such as mitotic nuclear division, extracellular matrix organization, and fibroblast migration. At the same time, these genes are also expressed in chromosomal regions, spindles, collagen trimers, and other cellular components. In addition, these genes also play a role in some critical signaling pathways, such as protein digestion and

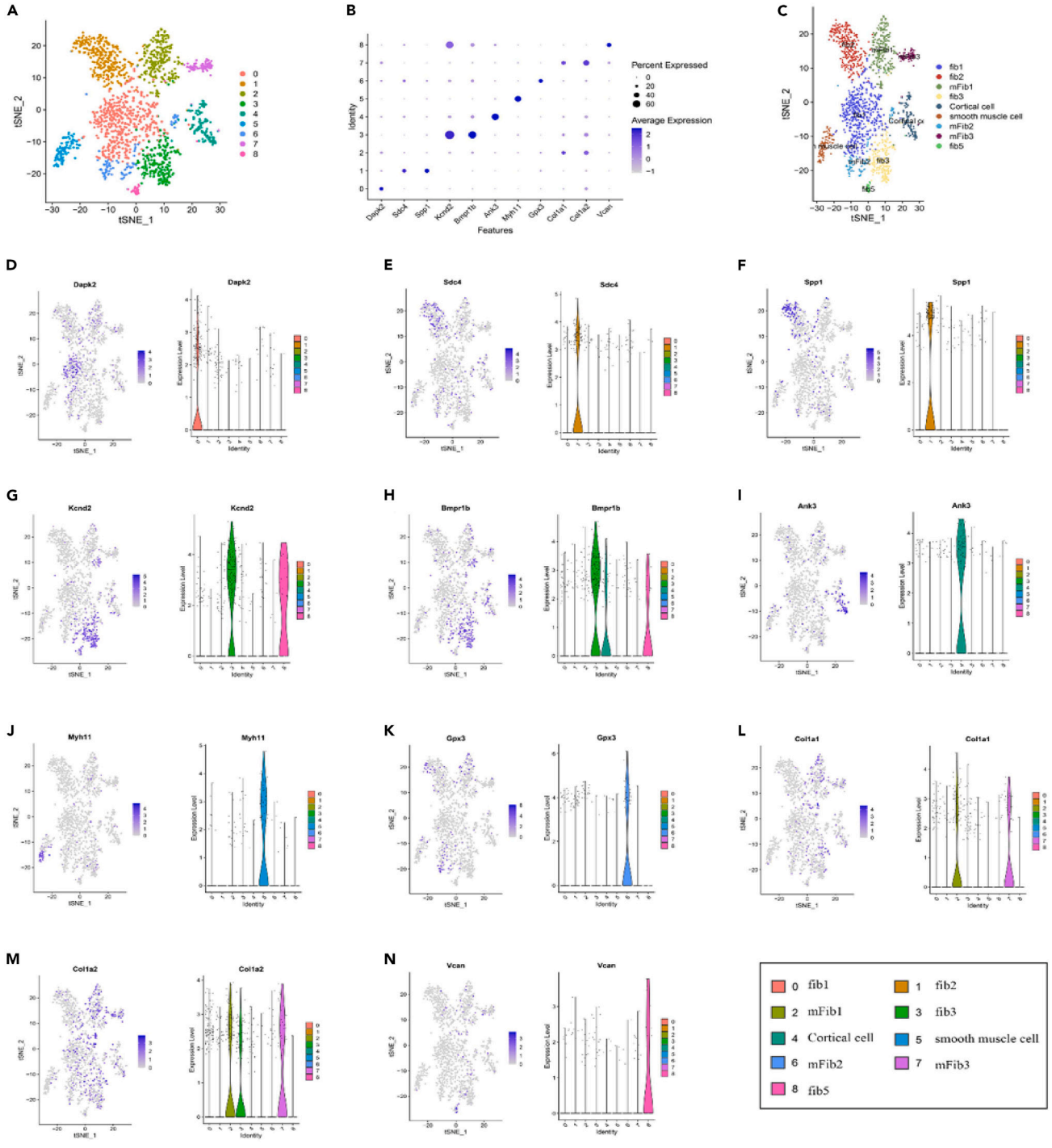

Figure 3. Analysis of Marker Gene Expression in Cell Clusters

(A) t-SNE cluster analysis classifying cells into 9 subclusters.

(B) Bubble plot showing the expression of hub genes in each cell cluster.

(C) Annotation of the 9 subclusters.

(D–N) Scatterplots (left) showing the expression of marker genes in each cell cluster, with darker blue color indicating higher average expression levels, and violin plots (right) showing the expression of marker genes in each cell cluster.

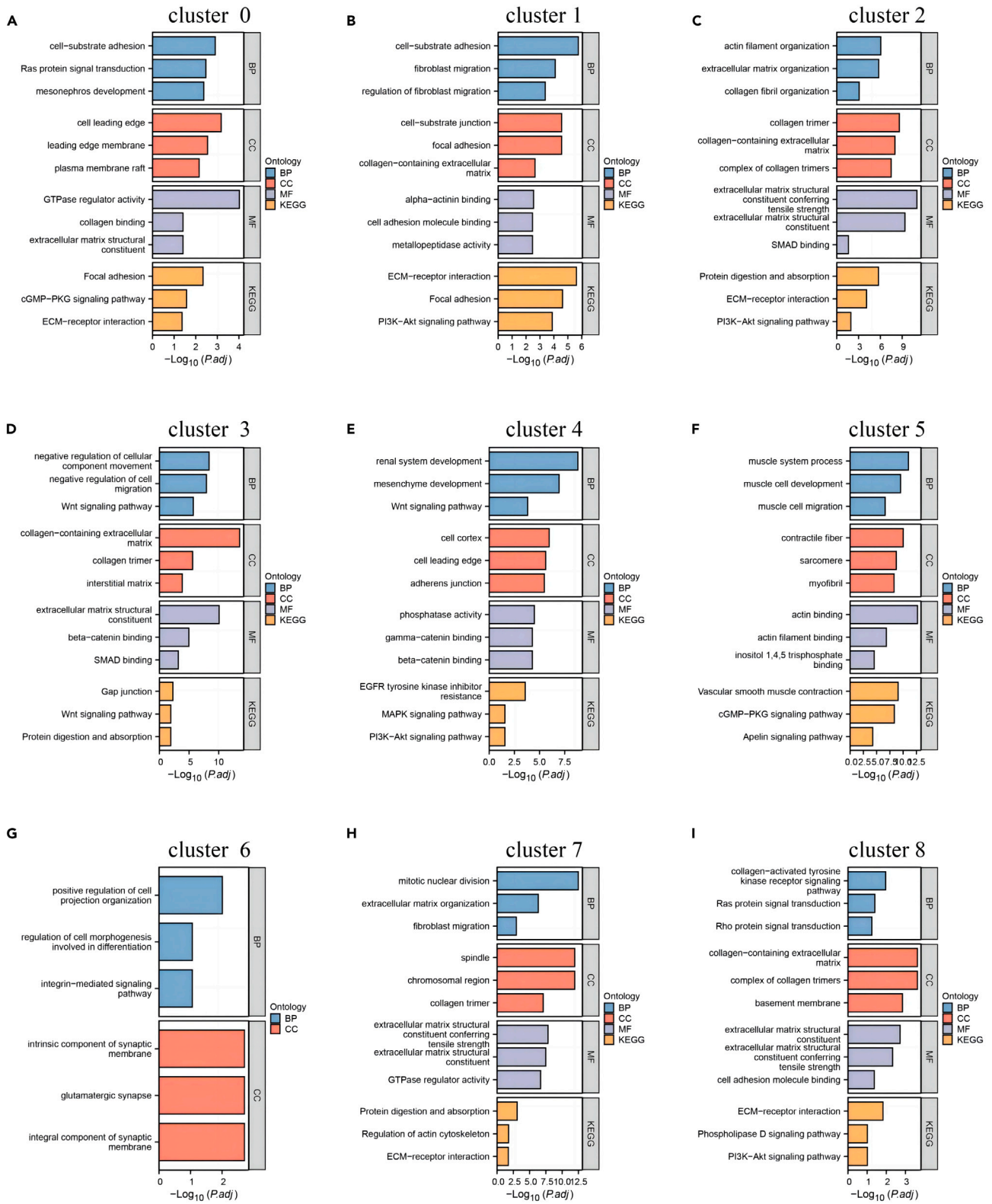

Figure 4. Functional Enrichment Analysis of Highly Expressed Genes in Each Cell Cluster

(A–I) GO-KEGG enrichment analysis of highly expressed genes in cell clusters; BP, CC, and MF represent Biological Process, Cellular Component, and Molecular Function, respectively.

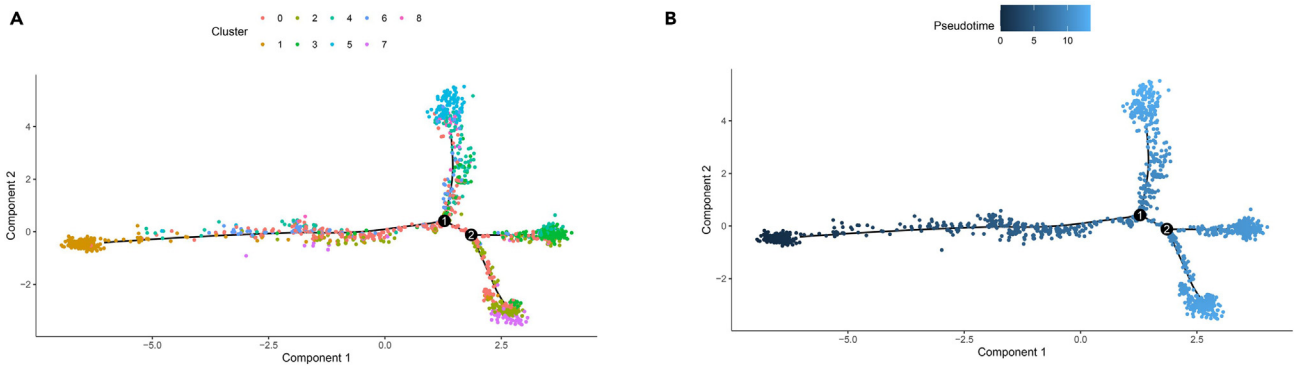

Figure 5. Identification of Temporal Changes in Cell Subpopulations
(A and B) Pseudotime analysis of fibroblast subpopulation.

absorption, regulation of actin cytoskeleton, and ECM-receptor interaction (Figure 4H). These enrichment results suggest that cells in cluster 7 may play a critical role in cell division, formation and function of the extracellular matrix, and migration of fibroblasts.

For cluster 8, we observed that its marker genes mainly involve critical biological processes such as collagen-activated tyrosine kinase receptor signaling pathway, Ras and Rho protein signal transduction, as well as functions in collagen trimer complex and collagen-containing extracellular matrix cellular components (Figure 4I). In addition, these genes are also involved in critical signaling pathways such as ECM-receptor interaction, PI3K-Akt signaling pathway, and phospholipase D signaling pathway. These enrichment results reveal the crucial roles of cluster 8 cells in cellular signal transduction, formation and function of extracellular matrix, and cell adhesion.

We conducted a pseudo-time analysis to investigate the dynamic changes and functional evolution of fibroblast subpopulations during renal fibrosis. As shown in Figures 5 and 9 cellular subpopulations were mapped to a standard "root" and three distinct branches. We found that clusters 0 and 1 are located at the starting end of the "root," indicating they may be the earliest formed cell subgroups. Subsequently, clusters 0 and 1 differentiated into other subgroups, forming clusters 5, 6, and 8 in the upper branch, clusters 2 and 7 in the upper branch, and clusters 3 and 4 on the right branch. Clusters 2 and 7 have formed in later stages.

The above results indicate that clusters 0 and 1 may play crucial roles in the early fibrosis stages and further differentiate into other subtypes of fibroblasts during the subsequent process. On the contrary, clusters 2 and 7 may play a dominant role in the later fibrosis stages.

Differential gene expression in ischemia-reperfusion injury mouse model reveals Spp1 as a potential biomarker for renal fibrosis progression

We established an ischemia-reperfusion injury (IRI) mouse model to investigate the effects of kidney damage. Total RNA was extracted from mouse kidneys 2 days after the IRI procedure and subjected to RNA-seq analysis. After data quality control and batch effect removal, differential gene expression analysis was performed using R software. Genes with $|\log FC| > 2$ and $p < 0.05$ were considered differentially expressed genes (DEGs). 328 DEGs were identified, including 246 upregulated genes and 82 downregulated genes (Figure 6A). The expression of differential genes is shown as a heatmap in Figure 6B, demonstrating a difference in gene expression between the IRI and the Sham groups.

To further explore the potential functions and roles of differentially expressed genes (DEGs), we conducted GO and KEGG enrichment analyses. GO enrichment analysis of DEGs revealed their involvement in various biological processes including nuclear division, cell-matrix adhesion, and collagen fibril organization. Additionally, they were associated with cellular components such as kinetochore, collagen-containing extracellular matrix, collagen trimer, and extracellular matrix structural constituents. Furthermore, the molecular functions of these DEGs included microtubule binding and cellular skeletal movement activity (Figure 6C). KEGG enrichment analysis further revealed their involvement in key pathways such as cell cycle, ECM-receptor interaction, and focal adhesion.

The results of the Metascape enrichment analysis revealed the potential roles of these 328 genes in numerous critical biological processes and signaling pathways. These genes are involved in regulating the cell cycle, tissue organization of the extracellular matrix, and the structure of collagen fibers, as well as the positive regulation of cell migration and matrix adhesion. Furthermore, they are also implicated in specific biological processes such as hemostasis, actin cytoskeleton organization, kinetochore organization, and supramolecular fiber assembly (Figure 6D). The interaction between the biological processes and signaling pathways enriched by DEGs is shown in Figure 6E.

Based on the enrichment analysis results from GO, KEGG, and Metascape, these factors are likely involved in regulating the cell cycle, organizing collagen fibers, integrating the structure of the extracellular matrix, and finely controlling cell migration and adhesion.[23,24]

We performed ElasticNet and LASSO regression analyses (Figures 7A and 7B) on these 328 differentially expressed genes (DEGs) and selected disease-related signature genes to identify critical genes impacting renal fibrosis. The prospective time series analysis revealed that cluster 0 and cluster 1 fibroblast subgroups may further differentiate into other fibroblast subgroups in kidney fibrosis formation. To screen for disease-associated genes expressed in fibroblasts, we took the intersection of the genes identified by ElasticNet and LASSO regression analysis with the marker genes for fibroblast subgroups cluster 0 or cluster 1.

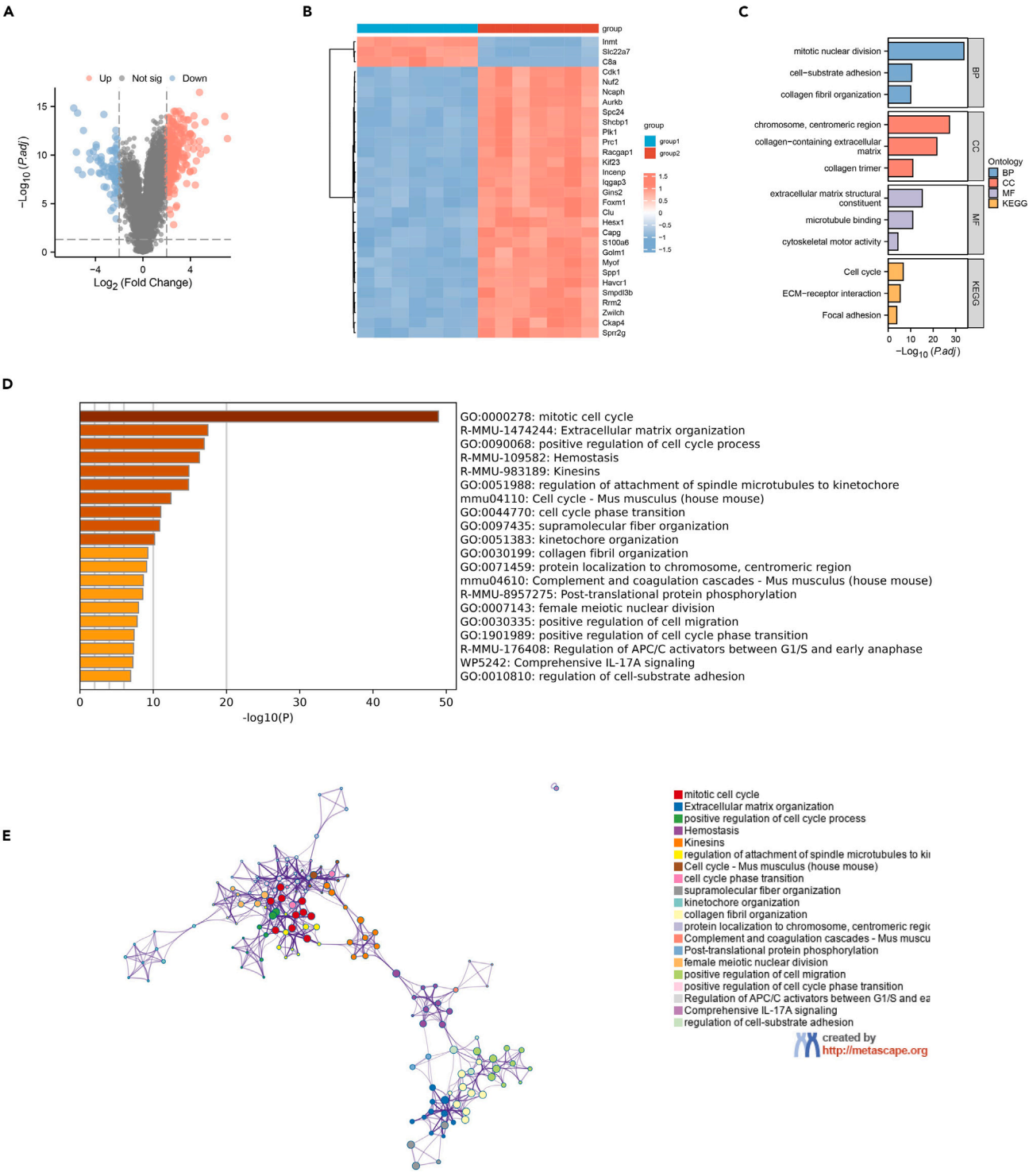

Figure 6. Functional Enrichment Analysis of Differentially Expressed Genes

(A) Volcano plot showing the differential gene expression of RNA-seq data, with blue dots representing downregulated genes, red dots representing upregulated genes, and black dots representing genes with no difference. The comparison is between 7 sham renal samples and 7 renal samples 2 days after IRI surgery.

(B) Heatmap showing the clustering of the top 30 differentially expressed genes.

(C) Bar plots showing GO and KEGG pathway enrichment analysis of DEGs at the Biological Process, Cellular Component, and Molecular Function levels.

(D and E) Metascape enrichment analysis results of DEGs and their corresponding interaction networks.

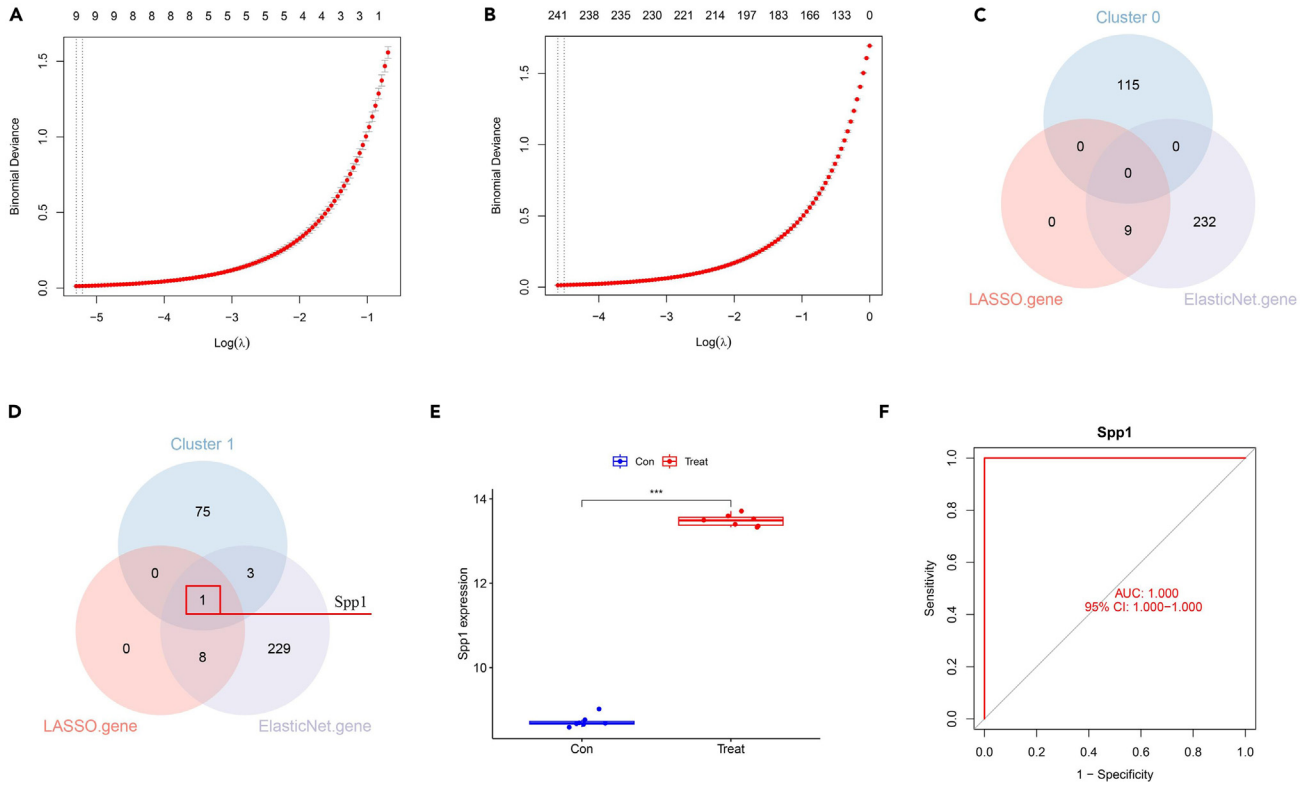

Figure 7. Identification of Kidney Fibrosis Feature Genes using Machine Learning Algorithms

(A and B) ElasticNet and LASSO coefficient selection plots.

(C and D) Venn diagrams showing the intersection analysis of feature genes selected by ElasticNet and LASSO regression analysis with cluster 0 and cluster 1 marker genes of fibroblast subpopulations.

(E) Boxplots showing the expression of Spp1 in the merged dataset.

(F) ROC curve plot showing the predictive value of Spp1 in kidney fibrosis diagnosis based on the merged dataset, with the Area Under the ROC Curve (AUC) ranging from 0 to 1, where a higher value indicates higher accuracy of the biomarker. CI represents the confidence interval of AUC. In all graphs, * represents $p < 0.05$, ** represents $p < 0.01$, and *** represents $p < 0.001$.

Intersection analysis results show no disease-associated genes in the marker genes of cluster 0 (Figure 7C), whereas the highly expressed gene Spp1 in cluster 1 is a disease-associated gene (Figure 7D). After investigating the expression of Spp1 in the merged dataset, we found that the expression level of Spp1 increased in the renal IRI group (Figure 7E). Further receiver operating characteristic (ROC) curve analysis showed a high correlation between Spp1 and renal fibrosis disease (AUC = 1.000, 95%CI = 1.000–1.000) (Figure 7F), suggesting that Spp1 might be a highly promising biomarker for effectively distinguishing renal fibrosis disease from a healthy state. Based on the above results, Spp1, as a highly expressed gene in cluster 1, may be associated with the early differentiation and activation of fibroblasts.

Spp1 potentiates renal fibrosis via the activation of the transforming growth factor-β/Smad signaling pathway in ischemia-reperfusion injury-Induced acute kidney injury model

A mouse model of acute kidney injury was established through ischemia-reperfusion injury (IRI) surgery. On the 2nd day and 1st week following the IRI surgery, blood samples of 6–8 mL were collected from the inferior vena cava, and the levels of creatinine (Cr) and blood urea nitrogen (BUN) were measured.[25–27] The levels of creatinine and blood urea nitrogen were significantly increased in the IRI_2d and IRI_1w groups of mice compared to the Sham group (Figures 8A and 8B). This result clearly demonstrated that ischemia-reperfusion surgery leads to kidney function impairment.

Secondly, we evaluated the impact of ischemia-reperfusion surgery on renal fibrosis using the Masson staining method. On the second day post-surgery, there was an increase in collagen fiber deposition in the renal tissue. By the seventh day post-surgery, this fibrotic change became even more pronounced (Figure 8I). These results indicate that ischemia-reperfusion surgery could induce renal fibrosis.

During the process of fibroblast-to-myofibroblast transition, the activation of the TGF-β/Smad signaling pathway is considered a crucial driving factor.[28,29] Therefore, we used the ELISA technique to measure the expression levels of critical components of the TGF-β/Smad signaling pathway and Spp1 in renal tissue.

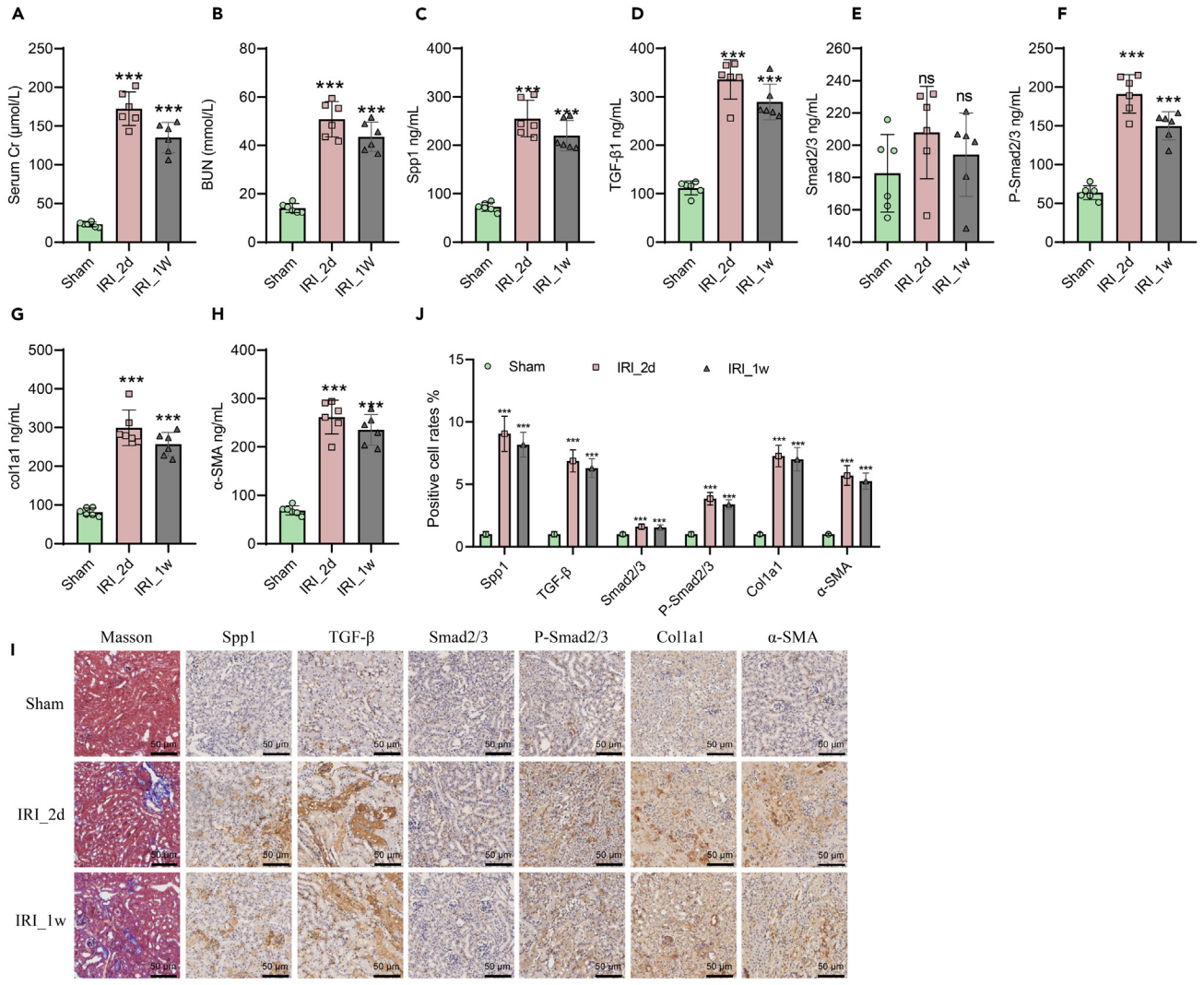

Figure 8. The impact of IRI surgery on renal physiological function and the expression levels of renal fibrosis-related factors in kidney tissue

(A and B) The effect of IRI surgery on renal function, where A shows the creatinine levels in the blood of mice in the Sham, IRI_2d, and IRI_1w groups; B shows the blood urea nitrogen levels in the blood of mice in the Sham, IRI_2d, and IRI_1w groups.

(C–H) Expression of Spp1, TGF-β, Smad2/3, P-Smad2/3, Col1a1, and α-SMA in kidney tissues using ELISA.

(I and J) Expression of Spp1, TGF-β, Smad2/3, P-Smad2/3, Col1a1, and α-SMA in kidney tissues using immunohistochemistry. In all the images, compared to the Sham group, * represents $p < 0.05$, ** represents $p < 0.01$, and *** represents $p < 0.001$; the bar in the image equals 750 μm.

The results revealed that on the second day following IRI surgery, there was a sustained increase in the expression levels of Spp1 and key components of the TGF-β/Smad signaling pathway, including TGF-β and P-Smad2/3. Simultaneously, there was a noticeable upregulation in the expression levels of critical markers involved in the fibroblast-to-myofibroblast differentiation process, such as Col1a1 (indicative of the degree of fibrosis) and α-SMA (reflecting the activation state of fibroblasts) (Figures 8C–8H). The results of immunohistochemistry also confirmed this point (Figures 8I and 8J).

In summary, our research findings indicate that Spp1 may influence fibroblast behavior and further impact the occurrence and development of renal fibrosis by participating in the activation of the TGF-β/Smad signaling pathway.[23,24]

Spp1 modulates fibroblast migration, proliferation, and differentiation in kidney interstitial cells

In order to obtain a purer population of fibroblasts, interstitial cells were isolated from the kidney and subsequently cultivated *in vitro* (Figure S3A). The effects of Spp1 knockdown and overexpression were evaluated using qPCR and western blot analyses (Figures S3B–S3D). The results showed that the Spp1 mRNA and protein levels in Spp1 knockdown fibroblasts (sh-Spp1-1 and sh-Spp1-2) were decreased. Among

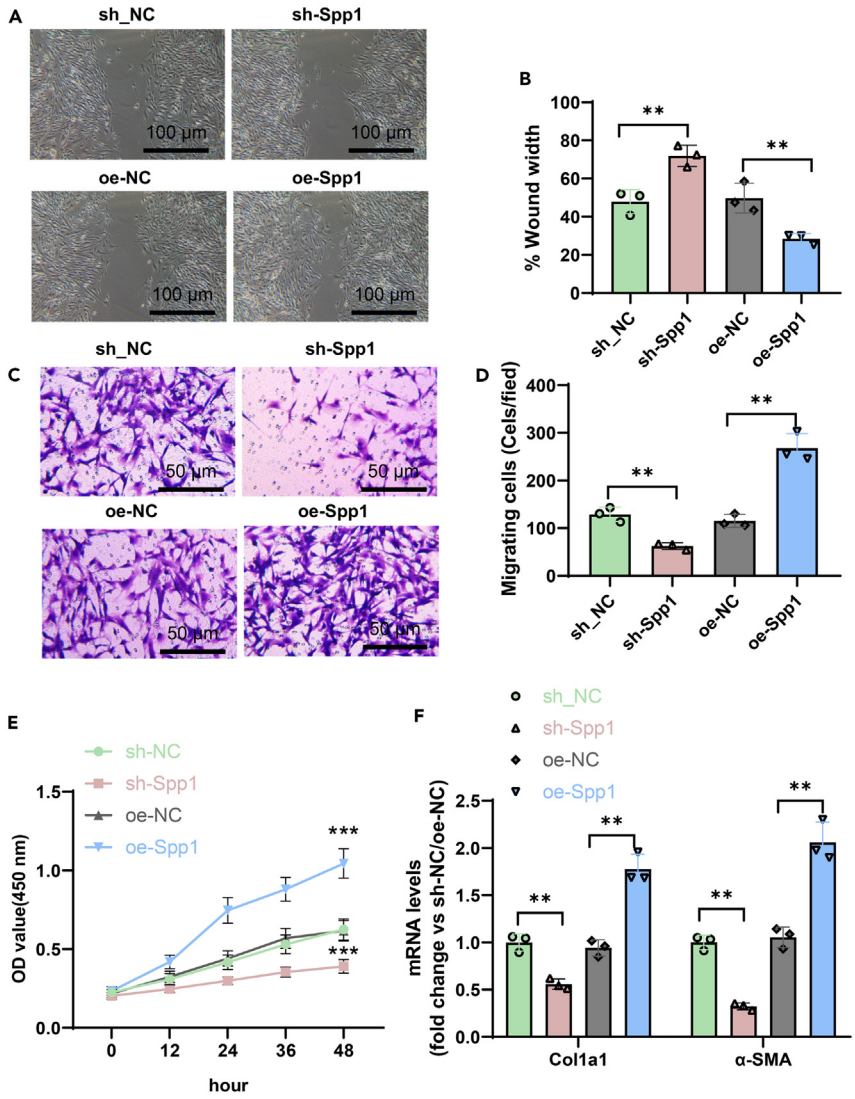

Figure 9. Investigation into the impact of Spp1 on fibroblast behavior

(A and B) Scratch experiment to evaluate the effect of Spp1 on fibroblast migration.

(C and D) Transwell chamber experiment to assess the effect of Spp1 on fibroblast migration.

(E) CCK8 experiment to measure the effect of Spp1 on fibroblast proliferation.

(F) qRT-PCR to detect the expression levels of Col1a1 and α-SMA in fibroblasts. In all the images, compared to the sh-NC or oe-NC groups, * represents $p < 0.05$, ** represents $p < 0.01$, and *** represents $p < 0.001$; bar in the image equals 750 μm or 500 μm; each experiment was conducted three times with six replicates each time.

them, the knockdown effect was more in sh-Spp1-1, so it was chosen as the sample for subsequent experiments. Similarly, in fibroblasts overexpressing Spp1 (oe-Spp1), both Spp1 mRNA and protein levels were upregulated, making it the choice for subsequent experiments.

The impact of Spp1 on fibroblast migration ability was assessed using scratch assays and Transwell chamber experiments. The findings revealed that knockdown of Spp1 decreased fibroblast migration capability, while the overexpression of Spp1 significantly enhanced fibroblast migration ability (Figures 9A–9D). Next, the impact of Spp1 on the proliferation capacity of fibroblasts was measured using CCK8 experiments. The results indicate that knockdown of Spp1 inhibits fibroblast proliferation, while the overexpression of Spp1 significantly enhances fibroblast proliferation (Figure 9E). Finally, the influence of Spp1 on the differentiation capacity of fibroblasts was assessed. The findings demonstrate that knockdown of Spp1 suppresses the expression of Col1a1 and α-SMA, whereas the overexpression of Spp1 promotes the expression of Col1a1 and α-SMA (Figure 9F).

The above experimental results indicate that Spp1 plays a vital role in regulating fibroblast behavior, including migration, proliferation, and differentiation.[23,24,30,31]

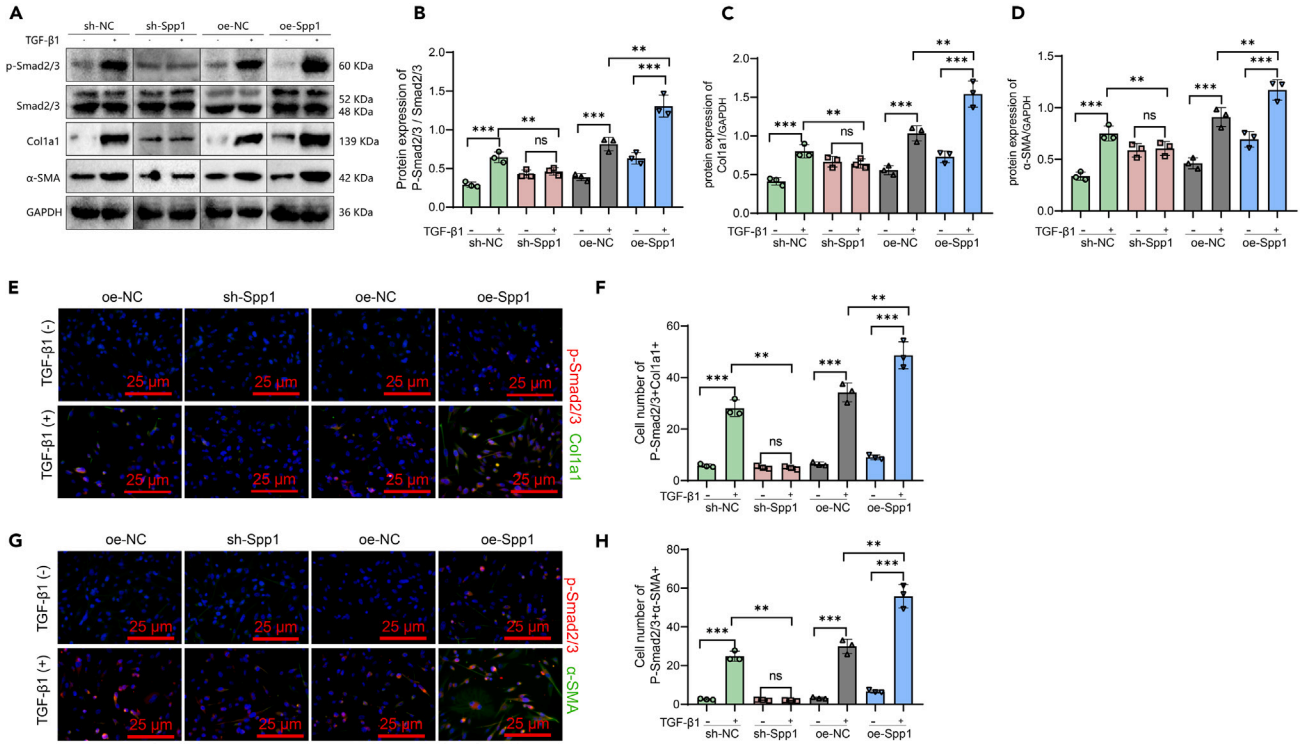

Figure 10. Molecular mechanism of Spp1 in regulating fibroblast behavior

(A) Western blot analysis of the effects of knocking down or overexpressing Spp1 on the expression of Smad2/3, Col1a1, and α-SMA under TGF-β induced conditions.

(B–D) Protein expression grayscale analysis to compare the expression and phosphorylation differences of the proteins.

(E–H) Double immunofluorescence staining of P-Smad2/3 (red) and Col1a1 (green) or α-SMA (green) to validate whether Spp1 regulates Col1a1 and α-SMA expression through the phosphorylation of Smad2/3. Blue represents cell nuclei stained with DAPI. In all the images, compared to the sh-NC or oe-NC groups, * represents $p < 0.05$, ** represents $p < 0.01$, and *** represents $p < 0.001$; bar equals 20 μm; each experiment was conducted three times with six replicates each time.

Spp1 regulates renal fibrosis through the modulation of transforming growth factor-β/Smad signaling in fibroblasts

We speculate that Spp1 may affect the behavior of fibroblasts and contribute to the occurrence and development of renal fibrosis, possibly through the activation of the TGF-β/Smad signaling pathway. To validate this hypothesis, we analyzed the effects of Spp1 knockdown/overexpression on the key components (Smad2/3) of the TGF-β/Smad signaling pathway under TGF-β-induced conditions. Western Blot results showed that knockdown of Spp1 inhibited the activation of Smad2/3 and decreased the expression levels of Col1a1 and α-SMA, markers of fibroblast differentiation, under TGF-β-induced conditions. In contrast, the overexpression of Spp1 promoted the phosphorylation of Smad2/3 and increased the expression of Col1a1 and α-SMA (Figures 10A–10D).

The results of immunofluorescence staining revealed that under TGF-β-induced conditions, knockdown of Spp1 decreased the number of P-Smad2/3+Col1a1+ and P-Smad2/3+α-SMA+ cells, while the overexpression of Spp1 increased the abundance of these cells (Figures 10E–10H).

Furthermore, we treated fibroblasts overexpressing Spp1 under TGF-β-induced conditions with A83-01, an inhibitor of Smad2/3 phosphorylation.[32] The experimental results showed that A83-01 significantly suppressed the elevated levels of Smad2/3 phosphorylation induced by Spp1 overexpression, as well as the upregulation of Col1a1 and α-SMA expression caused by Spp1 overexpression (Figure 11).

In conclusion, the influence of Spp1 on fibroblast behavior and its promotion of renal fibrosis have significant implications for renal physiological function. These effects are mediated through the regulation of Smad2/3 phosphorylation, a crucial factor in the TGF-β/Smad signaling pathway..[23,24,30,31]

Reduction of fibrosis degree in Spp1 knockout mice after renal ischemia reperfusion injury

The degree of fibrosis in Spp1 knockout mice is reduced after renal ischemia-reperfusion injury. To further verify the role of Spp1 in promoting renal fibrosis and affecting renal physiological function through the regulation of TGF-β/Smad signaling pathway key factor, Smad2/3 phosphorylation, we conducted *in vivo* validation experiments using Spp1−/− mice. Firstly, an acute kidney injury mouse model was successfully established through ischemia-reperfusion surgery (IRI). One week after the IRI surgery, we collected 6–8 mL of blood from the inferior vena

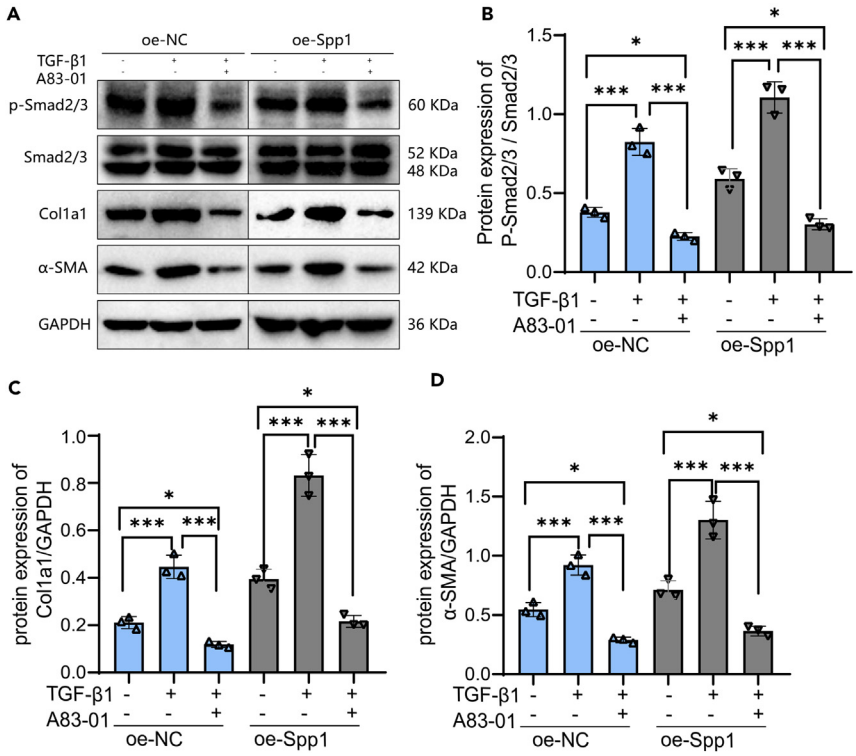

Figure 11. The effect of adding A83-01 inhibitor under TGF-β-induced conditions on fibroblast behavior

Note: (A) Western blot analysis of the effects of overexpressing Spp1 under TGF-β-induced conditions with or without adding A83-01 inhibitor on the expression of Smad2/3, P-Smad2/3, Col1a1, and α-SMA.

(B–D) Protein expression grayscale analysis to compare the expression and phosphorylation differences of the proteins. In all the images, * represents $p < 0.05$, ** represents $p < 0.01$, and *** represents $p < 0.001$; each experiment was conducted three times with six replicates each time.

cava and measured the levels of creatinine (Cr) and blood urea nitrogen (BUN) in the blood. Compared to the Spp1$^{+/+}$ surgery group, the Spp1−/− surgery group of mice showed a significant decrease in the levels of creatinine and blood urea nitrogen (Figures 12A and 12B). This result clearly indicates that knocking down Spp1 mitigates the damage to renal function caused by ischemia-reperfusion surgery.

We determined the expression levels of key components of the TGF-β/Smad signaling pathway as well as Spp1 in renal tissue using ELISA. The results showed that compared to the Spp1$^{+/+}$ group, the Spp1−/− group of mice had significantly reduced expression levels of Spp1 and key components of the TGF-β/Smad signaling pathway, including TGF-β and P-Smad2/3. At the same time, the expression levels of key markers for fibroblast differentiation into myofibroblasts, Col1a1 (indicative of the degree of fibrosis) and α-SMA (indicative of the activated state of fibroblasts), were also significantly decreased (Figures 12C–12H).

Next, we used Masson's staining to evaluate the impact of ischemia-reperfusion surgery on renal fibrosis. In Spp1$^{+/+}$ mice, significant renal fibrosis changes were observed one week after surgery (Figure 12I). On the other hand, the degree of renal fibrosis in the Spp1−/− surgery group of mice was milder. These results indicate that knocking down Spp1 can alleviate renal fibrosis induced by ischemia-reperfusion surgery. Immunohistochemistry was also conducted to detect the expression levels of key components of the TGF-β/Smad signaling pathway as well as Spp1 in renal tissue, yielding consistent results with ELISA (Figures 12I and 12J).

In summary, the results of our *in vivo* experiments demonstrate that Spp1, through its involvement in the activation of the TGF-β/Smad signaling pathway, influences the behavior of fibroblasts, thus further affecting the occurrence and development of renal fibrosis.

DISCUSSION

Renal fibrosis represents a multifaceted pathological process characterized by cellular and molecular interactions.[33] A pivotal determinant in this intricate dance is the transformation of fibroblasts into myofibroblasts, as myofibroblasts undertake the central role of primary cellular effectors driving the relentless march of fibrosis.[34] The present study embarked on a molecular exploration of kidney fibrosis, employing the precision of single-cell data analysis to adeptly anticipate marker genes intricately entwined with fibroblasts.[35] Notably, the Spp1 gene has assumed a spotlight, garnering substantial attention for its potential significance in orchestrating the behavior and fibrogenic voyage of fibroblasts.[36]

Spp1, also known as osteopontin, is a protein encoded by the OPN gene in humans. It is located on chromosome 4q21 and belongs to the SIBLING (Small Integrin-Binding Ligand N-linked Glycoprotein) family.[37] Osteopontin, the product of the Spp1 gene, is a

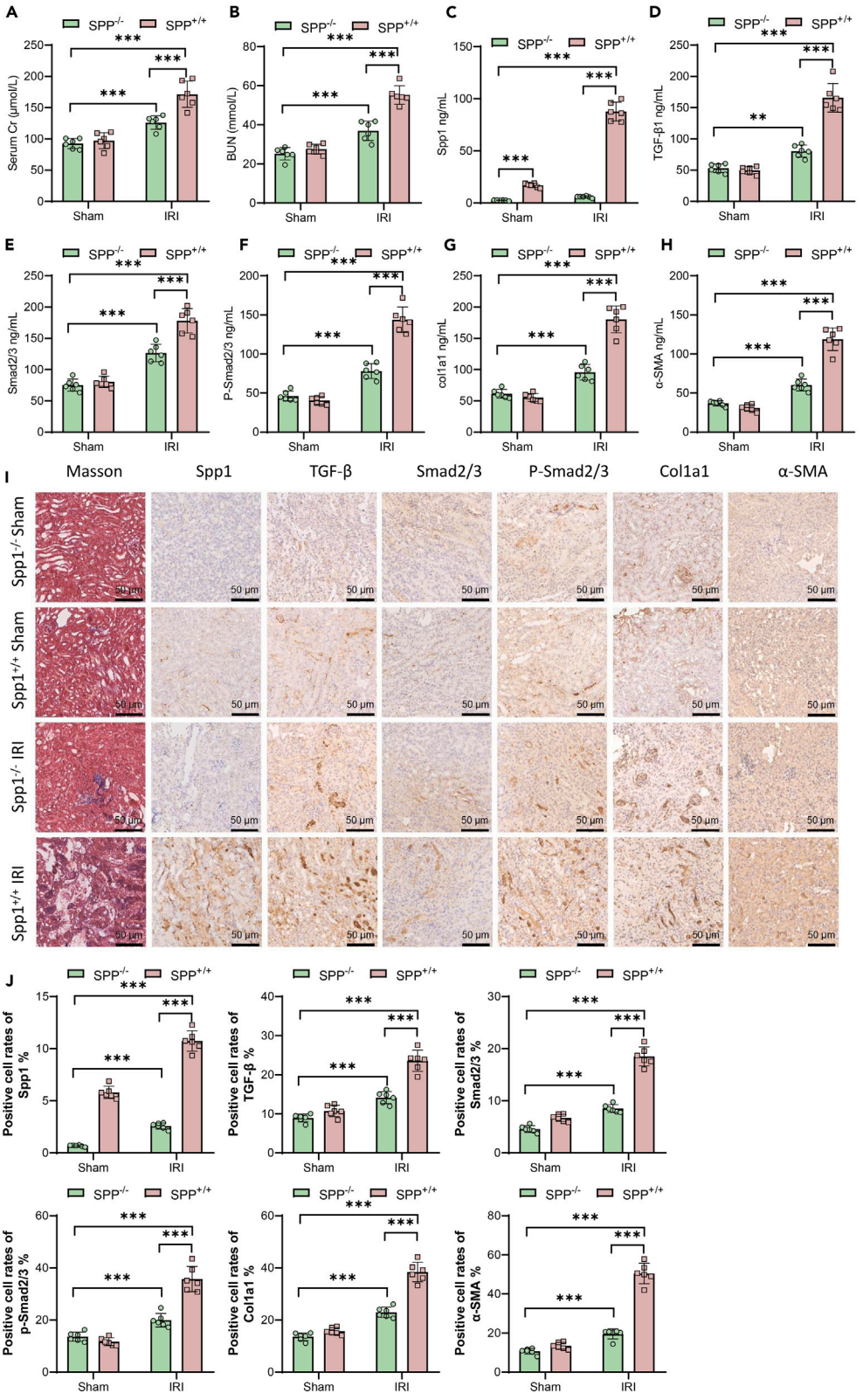
A
B
C
D
E
F
G
H
SPP-/-
SPP+/+
Serum Cr (μmol/L)
BUN (mmol/L)
Spp1 ng/mL
TGF-β1 ng/mL
Smad2/3 ng/mL
P-Smad2/3 ng/mL
col1a1 ng/mL
α-SMA ng/mL
Sham
IRI
I
Masson
Spp1
TGF-β
Smad2/3
P-Smad2/3
Col1a1
α-SMA
Spp1-/- Sham
Spp1+/+ Sham
Spp1-/- IRI
Spp1+/+ IRI
50 μm
J
Positive cell rates of Spp1 %
Positive cell rates of TGF-β %
Positive cell rates of Smad2/3 %
Positive cell rates of p-Smad2/3 %
Positive cell rates of Col1a1 %
Positive cell rates of α-SMA %

Figure 12. The impact of Spp1−/− mice on alleviating the effects of IRI surgery on renal physiological function and the expression levels of kidney fibrosis-related factors in their tissues

(A and B) The impact of IRI surgery on renal function. Panel A shows the creatinine levels in the blood of mice in each group. Panel B shows the urea nitrogen levels in the blood of mice in each group.

(C–H) Expression levels of Spp1, TGF-β, Smad2/3, P-Smad2/3, Col1a1, and α-SMA in kidney tissues using ELISA technique.

(I and J) Expression levels of Spp1, TGF-β, Smad2/3, P-Smad2/3, Col1a1, and α-SMA in kidney tissues using immunohistochemistry technique. In all the panels above, * represents $p < 0.05$ when comparing the two groups, ** represents $p < 0.01$, and *** represents $p < 0.001$; the bar in the figure equals 50 μm.

phosphoglycoprotein that participates in various physiological processes such as osteoclast attachment to mineralized bone matrix, wound healing, immune response, and tissue remodeling.[38,39] Spp1 is associated with fibrosis in several organs including idiopathic pulmonary fibrosis,[40] atrial fibrosis,[41] and non-alcoholic steatohepatitis fibrosis.[42] Dong and Ma conducted a study where they exposed wild-type mice and Spp1 gene knockout mice to a carbon nanotube environment, revealing the role of Spp1 protein in pulmonary fibrosis at varying degrees.[23] In our research, we performed an in-depth analysis of mouse kidney single-cell sequencing to analyze and interpret 16 cell types present in renal tissue. We further conducted a subclustering analysis focusing on significantly proportioned fibroblast cells to identify the key factor Spp1. Validation of the bioinformatics analysis was carried out using a mouse IRI model, providing the first evidence of fibroblast involvement in the mouse kidney model. Additionally, we explained the role of Spp1 in promoting fibroblast differentiation into myofibroblasts by regulating the TGF-β/Smad signaling pathway through the isolation of mouse kidney fibroblast cells, thus driving renal fibrosis. This study contributes to the existing knowledge by exploring how Spp1 regulates fibroblast differentiation into myofibroblasts, thereby driving the process of renal fibrosis and providing new insights into the molecular mechanisms of renal fibrosis. Through single-cell transcriptome sequencing, this research delves into cellular heterogeneity in renal fibrosis tissue, revealing the roles of different cell subpopulations in the fibrotic process and offering possibilities for personalized treatment.[43] We identified Spp1 as a potential therapeutic target that plays a key role in the TGF-β/Smad signaling pathway. Targeting Spp1 as a drug may bring new treatment strategies for patients with renal fibrosis.

The TGF-β/Smad signaling pathway assumes a paramount role in the realm of cellular biology, specifically in the orchestration of fundamental cellular phenomena encompassing cell proliferation, differentiation, and migration.[44] Within the intricate landscape of renal fibrosis, this signaling pathway emerges as a linchpin, as it directly governs the metamorphosis of fibroblasts into myofibroblasts, thereby instigating the inexorable march of fibrosis.[45] The empirical evidence gleaned from this investigative endeavor unequivocally substantiates the central role of Spp1 within this intricate narrative. Notably, the expression of Spp1 substantially accentuates the phosphorylation of pivotal actors, specifically Smad2/3, within the TGF-β/Smad signaling pathway, thereby setting the pathway into dynamic motion. These revelatory findings undeniably allude to the intricate nexus connecting Spp1 with renal fibrosis, as well as its potentiation of fibrotic advancement through the conduit of the TGF-β/Smad signaling pathway. Evidently, Spp1 assumes a pivotal mantle throughout the entire spectrum of the fibrotic process.[16]

In vitro cellular experiments provide an intricately controlled and intuitive platform for biomedical exploration, affording researchers the precision to assess molecular and cellular functionalities. In this study, an exhaustive examination of fibroblast behavior was conducted, accomplished by manipulating Spp1 expression through both knockdown and overexpression techniques. Importantly, the attenuation of Smad2/3 phosphorylation, achieved through the administration of the A83-01 inhibitor, substantially impeded fibroblast differentiation. This critical observation offers robust evidence for the central role of Spp1 in modulating the TGF-β/Smad signaling pathway. Intriguingly, the experimental findings underscore the profound impact of manipulating Spp1 expression—whether by diminishing or enhancing it—on fibroblast behavior. Furthermore, mechanistic investigations have unveiled that Spp1's primary mode of action centers on the facilitation of Smad2/3, pivotal factors within the TGF-β/Smad signaling cascade, through phosphorylation. The TGF-β/Smad pathway is renowned for its pivotal involvement in various biological processes, particularly the onset of fibrosis.[46] Notably, the outcomes reveal that following Spp1 overexpression, the introduction of the Smad2/3 phosphorylation inhibitor, A83-01, efficaciously retards fibroblast differentiation. This compelling outcome incontrovertibly underscores Spp1's role in expediting the transformation of fibroblasts into myofibroblasts by regulating the TGF-β/Smad signaling pathway. In sum, Spp1 not only emerges as intricately interwoven with fibroblast behavior but also as a promoter of renal fibrosis through its modulation of the TGF-β/Smad signaling pathway. Consequently, Spp1 looms as a promising target for prospective therapeutic strategies in renal fibrosis, heralding innovative approaches to patient care.[18]

However, fibrosis plays a crucial role in the tissue repair process. Upon tissue injury, cell factors such as interleukin (IL)-10, transforming growth factor (TGF)-β1, and osteopontin (Spp1) are extensively secreted, stimulating fibroblast proliferation and new matrix formation.[23] It can be argued that the initial fibrotic response is essential for tissue repair and organ integrity preservation.[47] However, chronic repetitive organ damage can lead to excessive fibrosis and continuous extracellular matrix (ECM) deposition, resulting in maladaptive remodeling and organ dysfunction.[18] Examples include cardiac fibrosis, pulmonary fibrosis, and hepatic fibrosis. Therefore, maintaining appropriate levels of fibrosis is highly important. Our study provides clues for myofibroblast differentiation, suggesting that targeting Spp1 could be a potential strategy to inhibit fibrogenesis. In daily living, adopting healthy habits and reducing the occurrence of chronic inflammation can minimize tissue and organ damage, thus lowering the risk of excessive fibrosis.

This study utilized single-cell sequencing technology to elucidate the cellular cluster characteristics in fibrotic renal tissue. We identified nine distinct subpopulations of fibroblasts, each with unique functional properties. These subpopulations play critical roles in extracellular matrix formation, signal transduction, glomerular development, and muscle system development, suggesting that fibroblasts may collectively drive the progression of renal fibrosis through complex interplay within a network of relationships.[48] Although current technological limitations prevent direct analysis of the communication network between these subpopulations, these findings provide important clues for future

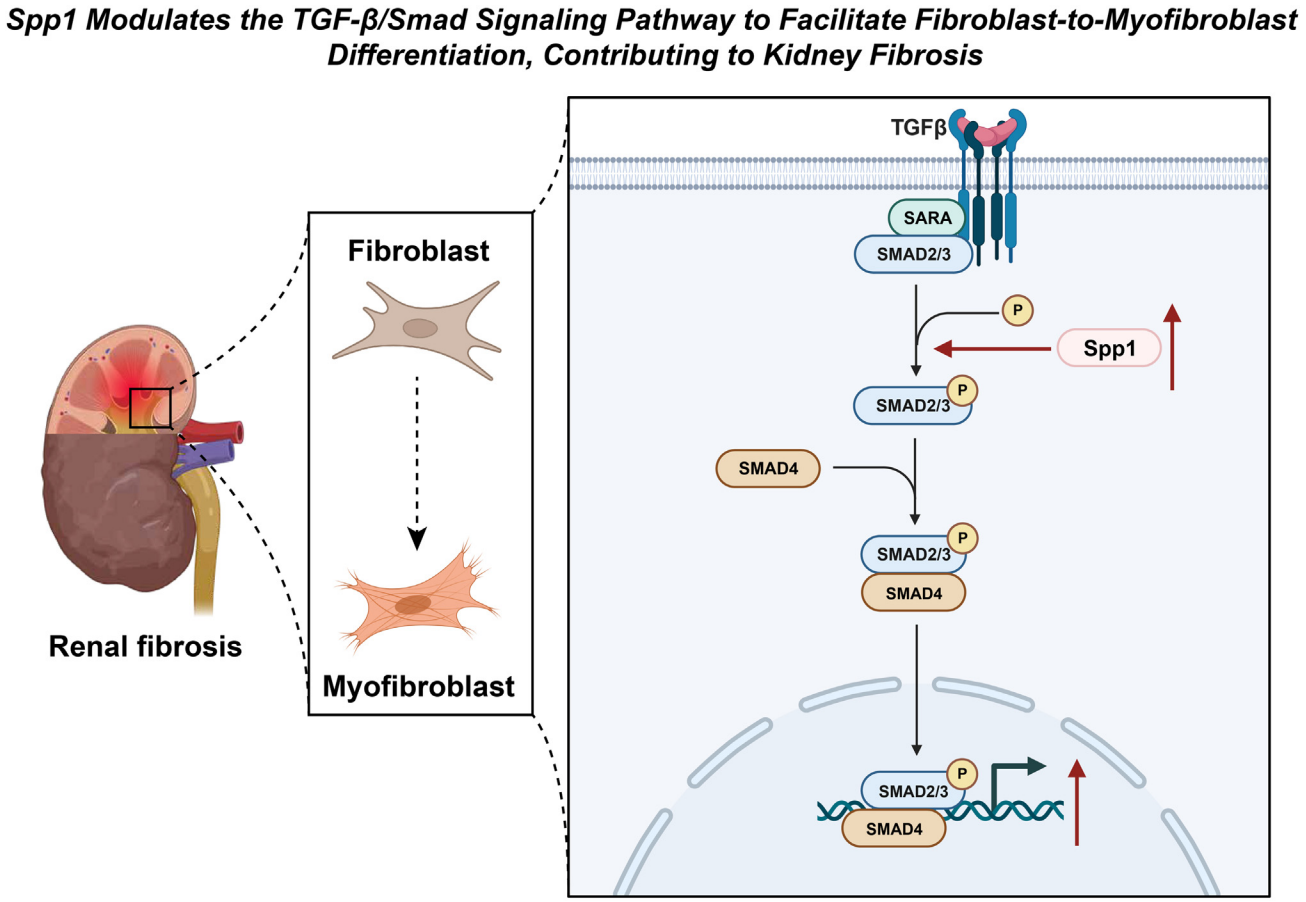

Figure 13. Molecular mechanism diagram illustrating how Spp1 regulates the TGF-β/Smad signaling pathway to promote fibroblast differentiation into myofibroblasts and drive renal fibrosis

research and hold promise for the development of new strategies for the treatment of renal fibrosis. Based on these results, we tentatively conclude that Spp1 regulates the TGF-β/Smad signaling pathway to promote fibroblast-to-myofibroblast differentiation, thereby driving renal fibrosis (Figure 13). Overall, our study not only provides new insights into the molecular mechanisms underlying renal fibrosis but also offers valuable clues for future therapeutic investigations. We hope that these findings will pave the way for more effective treatment methods for patients suffering from renal fibrosis.

Limitations of the study

While this study unveils significant insights into the molecular mechanisms driving kidney fibrosis, particularly through Spp1 and the TGF-β/Smad signaling pathway, it embodies inherent limitations. First, the reliance on animal models, predominantly mice, to infer human disease mechanisms might not fully encapsulate the complexity of renal fibrosis in humans. Secondly, although single-cell sequencing profoundly enriches our understanding of cellular heterogeneity and dynamics within fibrotic kidney tissue, the translational potential of these findings to clinical treatments requires further validation. Additionally, the study focuses on the Spp1 gene and its role within a specific signaling pathway, potentially overlooking other critical pathways and interactions that contribute to fibrosis. Future research should aim to explore these alternative mechanisms and verify the therapeutic implications of targeting Spp1 in diverse patient populations and in conjunction with other treatment strategies.

STAR★METHODS

Detailed methods are provided in the online version of this paper and include the following:

- KEY RESOURCES TABLE
- RESOURCE AVAILABILITY
  - Lead contact
  - Materials availability

Table 1. shRNA interference sequence

Name	shRNA Sequences(5′-3′)
sh-NC	CCTAAGGTTAAGTCGCCCTCG
sh-Spp1-1	GGACGACGATGATGACGATGA
sh-Spp1-2	GACCACATGGACGACGATGAT

- Data and code availability
- EXPERIMENTAL MODEL AND STUDY PARTICIPANT DETAILS
  - Animals
  - Cell lines
- METHOD DETAILS
  - Single-cell RNA sequencing analysis
  - Characterization and evolutionary dynamics of fibroblast subpopulations
  - Differential gene expression analysis in IRI mouse model
  - Immunohistochemical staining and ELISA assays
  - Isolation and cultivation of renal interstitial fibroblasts
  - Cell transfection
  - RT-qPCR, CCK-8, and western blot
  - Wound healing and transwell assays
  - Immunofluorescent staining
  - TGF-β1 treatments
- QUANTIFICATION AND STATISTICAL ANALYSIS
  - Single-cell data quantification
  - Statistical analysis in experimental studies

SUPPLEMENTAL INFORMATION

Supplemental information can be found online at https://doi.org/10.1016/j.isci.2024.109839.

ACKNOWLEDGMENTS

Funding: This study was supported by National Natural Science Foundation of China (82070734).

All animal experiments are conducted after obtaining the approval of the ethics review committee of Nanjing Medical University and strictly adhere to the regulations for animal welfare and experimental procedures.

AUTHOR CONTRIBUTIONS

HD conceived and designed research. ZDX performed experiments. YL interpreted results of experiments. QY analyzed data. JZL prepared figures. QS drafted paper. HD and ZDX edited and revised article. All authors read and approved final version of article.

DECLARATION OF INTERESTS

The authors declare that they have no competing interests.

Received: October 23, 2023
Revised: March 1, 2024
Accepted: April 25, 2024
Published: May 9, 2024

Table 2. RT-qPCR primer sequence

Gene	Primer sequence
Spp1 (mouse)	F 5′-TCCCTCGATGTCATCCCTGT-3′ R 5′-ATCACATCCGACTGATCGGC-3′
GAPDH (mouse)	F 5′- CATCACTGCCACCCAGAAGACTG -3′ R 5′- ATGCCAGTGAGCTTCCCGTTCAG -3′

F, forward; R, reverse.

REFERENCES

1. Yu, S.M.W., and Bonventre, J.V. (2020). Acute kidney injury and maladaptive tubular repair leading to renal fibrosis. Curr. Opin. Nephrol. Hypertens. *29*, 310–318. https://doi.org/10.1097/MNH.0000000000000605.
2. Wu, Y., Min, J., Ge, C., Shu, J., Tian, D., Yuan, Y., and Zhou, D. (2020). Interleukin 22 in Liver Injury, Inflammation and Cancer. Int. J. Biol. Sci. *16*, 2405–2413. https://doi.org/10.7150/ijbs.38925.
3. Langewisch, E., and Mannon, R.B. (2021). Chronic Allograft Injury. Clin. J. Am. Soc. Nephrol. *16*, 1723–1729. https://doi.org/10.2215/CJN.15590920.
4. Powell, E.E., Wong, V.W.S., and Rinella, M. (2021). Non-alcoholic fatty liver disease. Lancet (London, England) *397*, 2212–2224. https://doi.org/10.1016/S0140-6736(20)32511-3.
5. Mehrabani, D., Khajehahmadi, Z., Tajik, P., Tamadon, A., Rahmanifar, F., Ashraf, M., Tanideh, N., and Zare, S. (2019). Regenerative Effect of Bone Marrow-derived Mesenchymal Stem Cells in Thioacetamide-induced Liver Fibrosis of Rats. Arch. Razi Inst. *74*, 279–286. https://doi.org/10.22092/ari.2018.110029.1120.
6. Li, L., Fu, H., and Liu, Y. (2022). The fibrogenic niche in kidney fibrosis: components and mechanisms. Nat. Rev. Nephrol. *18*, 545–557. https://doi.org/10.1038/s41581-022-00590-z.
7. Luba, R., Martinez, S., Jones, J., Pravetoni, M., and Comer, S.D. (2023). Immunotherapeutic strategies for treating opioid use disorder and overdose. Expet Opin. Invest. Drugs *32*, 77–87. https://doi.org/10.1080/13543784.2023.2173062.
8. Miranda, M.Z., Lichner, Z., Szászi, K., and Kapus, A. (2021). MRTF: Basic Biology and Role in Kidney Disease. Int. J. Mol. Sci. *22*, 6040. https://doi.org/10.3390/ijms22116040.
9. Hu, B., Lelek, S., Spanjaard, B., El-Sammak, H., Simões, M.G., Mintcheva, J., Aliee, H., Schäfer, R., Meyer, A.M., Theis, F., et al. (2022). Origin and function of activated fibroblast states during zebrafish heart regeneration. Nat. Genet. *54*, 1227–1237. https://doi.org/10.1038/s41588-022-01129-5.
10. Miquelestorena-Standley, E., da Silva, A.V.V., Monnier, M., Chadet, S., Piollet, M., Héraud, A., Lemoine, R., Bochaton, T., Derumeaux, G., Roger, S., et al. (2023). Human peripheral blood mononuclear cells display a temporal evolving inflammatory profile after myocardial infarction and modify myocardial fibroblasts phenotype. Sci. Rep. *13*, 16745. https://doi.org/10.1038/s41598-023-44036-3.
11. Lu, Y.P., Wu, H.W., Zhu, T., Li, X.T., Zuo, J., Hasan, A.A., Reichetzeder, C., Delic, D., Yard, B., Klein, T., et al. (2022). Empagliflozin reduces kidney fibrosis and improves kidney function by alternative macrophage activation in rats with 5/6-nephrectomy. Biomed. Pharmacother. *156*, 113947. https://doi.org/10.1016/j.biopha.2022.113947.
12. Ma, Y., Shi, J., Wang, F., Li, S., Wang, J., Zhu, C., Li, L., Lu, H., Li, C., Yan, J., et al. (2019). MiR-130b increases fibrosis of HMC cells by regulating the TGF-β1 pathway in diabetic nephropathy. J. Cell. Biochem. *120*, 4044–4056. https://doi.org/10.1002/jcb.27688.
13. Doke, T., Abedini, A., Aldridge, D.L., Yang, Y.W., Park, J., Hernandez, C.M., Balzer, M.S., Shrestra, R., Coppock, G., Rico, J.M.I., et al. (2022). Single-cell analysis identifies the interaction of altered renal tubules with basophils orchestrating kidney fibrosis. Nat. Immunol. *23*, 947–959. https://doi.org/10.1038/s41590-022-01200-7.
14. Cai, X., Zheng, Y., Ren, F., Zhang, S., Wu, L., and Yao, Y. (2022). Secretory phosphoprotein 1 secreted by fibroblast-like synoviocytes promotes osteoclasts formation via PI3K/AKT signaling in collagen-induced arthritis. Biomed. Pharmacother. *155*, 113687. https://doi.org/10.1016/j.biopha.2022.113687.
15. Yu, X., Xiao, Q., Yu, X., Cheng, Y., Lin, H., and Xiang, Z. (2022). A network pharmacology-based study on the mechanism of astragaloside IV alleviating renal fibrosis through the AKT1/GSK-3β pathway. J. Ethnopharmacol. *297*, 115535. https://doi.org/10.1016/j.jep.2022.115535.
16. Qi, J., Sun, H., Zhang, Y., Wang, Z., Xun, Z., Li, Z., Ding, X., Bao, R., Hong, L., Jia, W., et al. (2022). Single-cell and spatial analysis reveal interaction of FAP^+ fibroblasts and $SPP1^+$ macrophages in colorectal cancer. Nat. Commun. *13*, 1742. https://doi.org/10.1038/s41467-022-29366-6.
17. Peng, D., Fu, M., Wang, M., Wei, Y., and Wei, X. (2022). Targeting TGF-β signal transduction for fibrosis and cancer therapy. Mol. Cancer *21*, 104. https://doi.org/10.1186/s12943-022-01569-x.
18. Hoeft, K., Schaefer, G.J.L., Kim, H., Schumacher, D., Bleckwehl, T., Long, Q., Klinkhammer, B.M., Peisker, F., Koch, L., Nagai, J., et al. (2023). Platelet-instructed $SPP1^+$ macrophages drive myofibroblast activation in fibrosis in a CXCL4-dependent manner. Cell Rep. *42*, 112131. https://doi.org/10.1016/j.celrep.2023.112131.
19. Yeh, R., Dercle, L., Garg, I., Wang, Z.J., Hough, D.M., and Goenka, A.H. (2018). The Role of 18F-FDG PET/CT and PET/MRI in Pancreatic Ductal Adenocarcinoma. Abdom. Radiol. *43*, 415–434. https://doi.org/10.1007/s00261-017-1374-2.
20. Kuppe, C., Ibrahim, M.M., Kranz, J., Zhang, X., Ziegler, S., Perales-Patón, J., Jansen, J., Reimer, K.C., Smith, J.R., Dobie, R., et al. (2021). Decoding myofibroblast origins in human kidney fibrosis. Nature *589*, 281–286. https://doi.org/10.1038/s41586-020-2941-1.
21. Yuan, Q., Tan, R.J., and Liu, Y. (2019). Myofibroblast in Kidney Fibrosis: Origin, Activation, and Regulation. Adv. Exp. Med. Biol. *1165*, 253–283. https://doi.org/10.1007/978-981-13-8871-2_12.
22. Lynch, M.D., and Watt, F.M. (2018). Fibroblast heterogeneity: implications for human disease. J. Clin. Invest. *128*, 26–35. https://doi.org/10.1172/JCI93555.
23. Dong, J., and Ma, Q. (2017). Osteopontin enhances multi-walled carbon nanotube-triggered lung fibrosis by promoting TGF-β1 activation and myofibroblast differentiation. Part. Fibre Toxicol. *14*, 18. https://doi.org/10.1186/s12989-017-0198-0.
24. Liu, J., Kumar, S., Dolzhenko, E., Alvarado, G.F., Guo, J., Lu, C., Chen, Y., Li, M., Dessing, M.C., Parvez, R.K., et al. (2017). Molecular characterization of the transition from acute to chronic kidney injury following ischemia/reperfusion. JCI Insight *2*, e94716. https://doi.org/10.1172/jci.insight.94716.
25. Li, X., Peng, X., Qiao, B., Peng, M., Deng, N., Yu, R., and Tan, Z. (2022). Gut-Kidney Impairment Process of Adenine Combined with Folium sennae-Induced Diarrhea: Association with Interactions between Lactobacillus intestinalis, Bacteroides acidifaciens and Acetic Acid, Inflammation, and Kidney Function. Cells *11*, 3261. https://doi.org/10.3390/cells11203261.
26. Wei, C., Zhao, S., Zhang, Y., Gu, W., Kumar Sarker, S., Liu, S., Li, B., Wang, X., Li, Y., and Wang, X. (2021). Effect of Multiple-Nutrient Supplement on Muscle Damage, Liver, and Kidney Function After Exercising Under Heat: Based on a Pilot Study and a Randomised Controlled Trial. Front. Nutr. *8*, 740741. https://doi.org/10.3389/fnut.2021.740741.
27. Hamidianshirazi, M., Shafiee, M., Ekramzadeh, M., Torabi Jahromi, M., and Nikaein, F. (2023). Diet therapy along with nutrition education can improve renal function in people with stages 3-4 chronic kidney disease who do not have diabetes: a randomised controlled trial. Br. J. Nutr. *129*, 1877–1887. https://doi.org/10.1017/S0007114522002094.
28. Jung, S.W., Kim, S.M., Kim, A., Park, S.H., Moon, J.Y., and Lee, S.H. (2022). Midbody plays an active role in fibroblast-myofibroblast transition by mediating TGF-β signaling. FASEB J. *36*, e22272. https://doi.org/10.1096/fj.202101613R.
29. Ma, H., Duan, X., Zhang, R., Li, H., Guo, Y., Tian, Y., Huang, M., Chen, G., Wang, Z., and Li, L. (2022). Loureirin A Exerts Antikeloid Activity by Antagonizing the TGF-β1/Smad Signalling Pathway. Evid. Based. Complement. Alternat. Med. *2022*, 8661288. https://doi.org/10.1155/2022/8661288.
30. Lenga, Y., Koh, A., Perera, A.S., McCulloch, C.A., Sodek, J., and Zohar, R. (2008). Osteopontin expression is required for myofibroblast differentiation. Circ. Res. *102*, 319–327. https://doi.org/10.1161/CIRCRESAHA.107.160408.
31. Eun, J.W., Yoon, J.H., Ahn, H.R., Kim, S., Kim, Y.B., Lim, S.B., Park, W., Kang, T.W., Baek, G.O., Yoon, M.G., et al. (2023). Cancer-associated fibroblast-derived secreted phosphoprotein 1 contributes to resistance of hepatocellular carcinoma to sorafenib and lenvatinib. Cancer Commun. *43*, 455–479. https://doi.org/10.1002/cac2.12414.
32. Wu, Y., Tran, T., Dwabe, S., Sarkissyan, M., Kim, J., Nava, M., Clayton, S., Pietras, R., Farias-Eisner, R., and Vadgama, J.V. (2017). A83-01 inhibits TGF-β-induced upregulation of Wnt3 and epithelial to mesenchymal transition in HER2-overexpressing breast cancer cells. Breast Cancer Res. Treat. *163*, 449–460. https://doi.org/10.1007/s10549-017-4211-y.
33. Calle, P., and Hotter, G. (2020). Macrophage Phenotype and Fibrosis in Diabetic Nephropathy. Int. J. Mol. Sci. *21*, 2806. https://doi.org/10.3390/ijms21082806.
34. Zhou, Y., Li, M., Shen, T., Yang, T., Shi, G., Wei, Y., Chen, C., Wang, D., Wang, Y., and Zhang, T. (2022). Celastrol Targets Cullin-Associated and Neddylation-Dissociated 1 to Prevent Fibroblast-Myofibroblast Transformation against Pulmonary Fibrosis. ACS Chem. Biol. *17*, 2734–2743. https://doi.org/10.1021/acschembio.2c00099.
35. Bai, Y.M., Yang, F., Luo, P., Xie, L.L., Chen, J.H., Guan, Y.D., Zhou, H.C., Xu, T.F., Hao, H.W., Chen, B., et al. (2023). Single-cell transcriptomic dissection of the cellular and molecular events underlying the triclosan-induced liver fibrosis in mice. Mil. Med. Res. *10*, 7. https://doi.org/10.1186/s40779-023-00441-3.
36. Månberg, A., Skene, N., Sanders, F., Trusohamn, M., Remnestål, J., Szczepińska,

A., Aksoylu, I.S., Lönnerberg, P., Ebarasi, L., Wouters, S., et al. (2021). Altered perivascular fibroblast activity precedes ALS disease onset. Nat. Med. *27*, 640–646. https://doi.org/10.1038/s41591-021-01295-9.

37. Martín-Márquez, B.T., Sandoval-García, F., Corona-Meraz, F.I., Martínez-García, E.A., Sánchez-Hernández, P.E., Salazar-Páramo, M., Fletes-Rayas, A.L., González-Inostroz, D., and Vazquez-Del Mercado, M. (2023). Osteopontin: A Bone-Derived Protein Involved in Rheumatoid Arthritis and Osteoarthritis Immunopathology. Biomolecules *13*, 502. https://doi.org/10.3390/biom13030502.
38. Bandopadhyay, M., Bulbule, A., Butti, R., Chakraborty, G., Ghorpade, P., Ghosh, P., Gorain, M., Kale, S., Kumar, D., Kumar, S., et al. (2014). Osteopontin as a therapeutic target for cancer. Expert Opin. Ther. Targets *18*, 883–895. https://doi.org/10.1517/14728222.2014.925447.
39. Kahles, F., Findeisen, H.M., and Bruemmer, D. (2014). Osteopontin: A novel regulator at the cross roads of inflammation, obesity and diabetes. Mol. Metabol. *3*, 384–393. https://doi.org/10.1016/j.molmet.2014.03.004.
40. Morse, C., Tabib, T., Sembrat, J., Buschur, K.L., Bittar, H.T., Valenzi, E., Jiang, Y., Kass, D.J., Gibson, K., Chen, W., et al. (2019). Proliferating SPP1/MERTK-expressing macrophages in idiopathic pulmonary fibrosis. Eur. Respir. J. *54*, 1802441. https://doi.org/10.1183/13993003.02441-2018.
41. Du, X., Liu, T., Shen, C., He, B., Feng, M., Liu, J., Zhuo, W., Fu, G., Wang, B., Xu, Y., and Chu, H. (2022). Anti-fibrotic mechanism of SPP1 knockdown in atrial fibrosis associates with inhibited mitochondrial DNA damage and TGF-β/SREBP2/PCSK9 signaling. Cell Death Dis. *8*, 246. https://doi.org/10.1038/s41420-022-00895-9.
42. Wang, C., Ren, Y.L., Zhai, J., Zhou, X.Y., and Wu, J. (2019). Down-regulated LAMA4 inhibits oxidative stress-induced apoptosis of retinal ganglion cells through the MAPK signaling pathway in rats with glaucoma. Cell Cycle *18*, 932–948. https://doi.org/10.1080/15384101.2019.1593645.
43. Deng, C.C., Hu, Y.F., Zhu, D.H., Cheng, Q., Gu, J.J., Feng, Q.L., Zhang, L.X., Xu, Y.P., Wang, D., Rong, Z., and Yang, B. (2021). Single-cell RNA-seq reveals fibroblast heterogeneity and increased mesenchymal fibroblasts in human fibrotic skin diseases. Nat. Commun. *12*, 3709. https://doi.org/10.1038/s41467-021-24110-y.
44. Lee, J.H., and Massagué, J. (2022). TGF-β in developmental and fibrogenic EMTs. Semin. Cancer Biol. *86*, 136–145. https://doi.org/10.1016/j.semcancer.2022.09.004.
45. Chen, C.H., Ke, G.M., Lin, P.C., and Lin, K.D. (2021). Therapeutic DNA vaccine encoding CEMIP (KIAA1199) ameliorates kidney fibrosis in obesity through inhibiting the Wnt/β-catenin pathway. Biochim. Biophys. Acta Gen. Subj. *1865*, 130019. https://doi.org/10.1016/j.bbagen.2021.130019.
46. Zhang, Q.F., Li, J., Jiang, K., Wang, R., Ge, J.L., Yang, H., Liu, S.J., Jia, L.T., Wang, L., and Chen, B.L. (2020). CDK4/6 inhibition promotes immune infiltration in ovarian cancer and synergizes with PD-1 blockade in a B cell-dependent manner. Theranostics *10*, 10619–10633. https://doi.org/10.7150/thno.44871.
47. Yang, H.W., Park, J.H., Jo, M.S., Shin, J.M., Kim, D.W., and Park, I.H. (2022). Eosinophil-Derived Osteopontin Induces the Expression of Pro-Inflammatory Mediators and Stimulates Extracellular Matrix Production in Nasal Fibroblasts: The Role of Osteopontin in Eosinophilic Chronic Rhinosinusitis. Front. Immunol. *13*, 777928. https://doi.org/10.3389/fimmu.2022.777928.
48. Liu, Y. (2011). Cellular and molecular mechanisms of renal fibrosis. Nat. Rev. Nephrol. *7*, 684–696. https://doi.org/10.1038/nrneph.2011.149.
49. Ma, L., Hernandez, M.O., Zhao, Y., Mehta, M., Tran, B., Kelly, M., Rae, Z., Hernandez, J.M., Davis, J.L., Martin, S.P., et al. (2019). Tumor Cell Biodiversity Drives Microenvironmental Reprogramming in Liver Cancer. Cancer Cell *36*, 418–430.e6. https://doi.org/10.1016/j.ccell.2019.08.007.
50. Arunachalam, D., Ramanathan, S.M., Menon, A., Madhav, L., Ramaswamy, G., Namperumalsamy, V.P., Prajna, L., and Kuppamuthu, D. (2022). Expression of immune response genes in human corneal epithelial cells interacting with Aspergillus flavus conidia. BMC Genom. *23*, 5. https://doi.org/10.1186/s12864-021-08218-5.
51. Linkner, T.R., Ambrus, V., Kunkli, B., Szojka, Z.I., Kalló, G., Csősz, É., Kumar, A., Emri, M., Tőzsér, J., and Mahdi, M. (2021). Cellular Proteo-Transcriptomic Changes in the Immediate Early-Phase of Lentiviral Transduction. Microorganisms *9*, 2207. https://doi.org/10.3390/microorganisms9112207.
52. Deng, Y.J., Ren, E.H., Yuan, W.H., Zhang, G.Z., Wu, Z.L., and Xie, Q.Q. (2020). GRB10 and E2F3 as Diagnostic Markers of Osteoarthritis and Their Correlation with Immune Infiltration. Diagnostics *10*, 171. https://doi.org/10.3390/diagnostics10030171.
53. Peng, X.Y., Wang, Y., Hu, H., Zhang, X.J., and Li, Q. (2019). Identification of the molecular subgroups in coronary artery disease by gene expression profiles. J. Cell. Physiol. *234*, 16540–16548. https://doi.org/10.1002/jcp.28324.
54. Guo, C., Gao, Y.Y., Ju, Q.Q., Zhang, C.X., Gong, M., and Li, Z.L. (2021). The landscape of gene co-expression modules correlating with prognostic genetic abnormalities in AML. J. Transl. Med. *19*, 228. https://doi.org/10.1186/s12967-021-02914-2.
55. Jiang, L., Zhang, M., Wu, J., Wang, S., Yang, X., Yi, M., Zhang, X., and Fang, X. (2020). Exploring diagnostic m6A regulators in endometriosis. Aging *12*, 25916–25938. https://doi.org/10.18632/aging.202163.
56. Ling, Z., Liu, Y., Wang, Z., Zhang, Z., Chen, B., Yang, J., Zeng, B., Gao, Y., Jiang, C., Huang, Y., et al. (2021). Single-Cell RNA-Seq Analysis Reveals Macrophage Involved in the Progression of Human Intervertebral Disc Degeneration. Front. Cell Dev. Biol. *9*, 833420. https://doi.org/10.3389/fcell.2021.833420.
57. Cheng, R., Chen, Y., Zhou, H., Wang, B., Du, Q., and Chen, Y. (2018). B7-H3 expression and its correlation with clinicopathologic features, angiogenesis, and prognosis in intrahepatic cholangiocarcinoma. APMIS *126*, 396–402. https://doi.org/10.1111/apm.12837.
58. Zhou, K.X., Huang, S., Hu, L.P., Zhang, X.L., Qin, W.T., Zhang, Y.L., Yao, L.L., Yu, Y., Zhou, Y.Q., Zhu, L., et al. (2021). Increased Nuclear Transporter KPNA2 Contributes to Tumor Immune Evasion by Enhancing PD-L1 Expression in PDAC. J. Immunol. Res. *2021*, 6694392. https://doi.org/10.1155/2021/6694392.
59. Luo, A., Zhou, X., Shi, X., Zhao, Y., Men, Y., Chang, X., Chen, H., Ding, F., Li, Y., Su, D., et al. (2019). Exosome-derived miR-339-5p mediates radiosensitivity by targeting Cdc25A in locally advanced esophageal squamous cell carcinoma. Oncogene *38*, 4990–5006. https://doi.org/10.1038/s41388-019-0771-0.
60. Lu, J., Liu, Q.H., Wang, F., Tan, J.J., Deng, Y.Q., Peng, X.H., Liu, X., Zhang, B., Xu, X., and Li, X.P. (2018). Exosomal miR-9 inhibits angiogenesis by targeting MDK and regulating PDK/AKT pathway in nasopharyngeal carcinoma. J. Exp. Clin. Cancer Res. *37*, 147. https://doi.org/10.1186/s13046-018-0814-3.
61. Chen, L., Qing, J., Xiao, Y., Huang, X., Chi, Y., and Chen, Z. (2022). TIM-1 promotes proliferation and metastasis, and inhibits apoptosis, in cervical cancer through the PI3K/AKT/p53 pathway. BMC Cancer *22*, 370. https://doi.org/10.1186/s12885-022-09386-7.
62. Nishizawa, Y. (2017). Refined quadratic estimations of Shafer's inequality. J. Inequalities Appl. *2017*, 40. https://doi.org/10.1186/s13660-017-1312-4.
63. Liu, J.Y. (2015). PE-Swab Direct STR Amplification of Forensic Touch DNA Samples. J. Forensic Sci. *60*, 693–701. https://doi.org/10.1111/1556-4029.12705.
64. Chen, G., Li, X., Zhu, H., Wu, H., He, D., Shi, L., Wei, F., Liu, X., Chen, N., and Liu, S. (2022). Transplanting neurofibromatosis-1 gene knockout neural stem cells improve functional recovery in rats with spinal cord injury by enhancing the mTORC2 pathway. Exp. Mol. Med. *54*, 1766–1777. https://doi.org/10.1038/s12276-022-00850-9.

STAR★METHODS

KEY RESOURCES TABLE

REAGENT or RESOURCE	SOURCE	IDENTIFIER
Antibodies		
Anti-Spp1 antibody	Solarbio, China	K200110M
Anti-Col1a1 antibody	Thermo Fisher, USA	PA5-29569
Anti-α-SMA antibody	Abcam, Cambridge, UK	ab5694
Anti-TGF-β1 antibody	Abcam, Cambridge, UK	ab215715
Anti-P-Smad2/3 antibody	Affbiotech, China	AF3367
Anti-Smad2/3 antibody	Affbiotech, China	AF6367
Anti-β-actin antibody	Abcam, UK	ab8226
Anti-P-Smad2/3 antibody	Cell Signaling, USA	8828
Anti-Smad2/3 antibody	Cell Signaling, USA	8685
Goat Anti-Rabbit Secondary Antibody	Beyotime, China	A0277
Alexa Fluor 647 Goat Anti-Rabbit Antibody	Solarbio, China	K0034G-AF647
FITC Goat Anti-Rat Secondary Antibody	GeneTex, USA	GTCX73
Custom Anti-P-Smad2/3 antibody (Rat, reactive with Mouse)	AbioCenter, China	Custom
Chemicals, peptides, and recombinant proteins		
Masson Trichrome Staining Kit	Solarbio, China	G1340
A83-01	ApexBio, USA	A3133
CCK-8 Assay Kit	Abcam, USA	ab228554
Penicillin	Solarbio, China	YZ-130437
Streptomycin	Solarbio, China	SS8800
Fetal Bovine Serum (FBS)	Solarbio, China	11011-8611
α-FGF	Abcam, UK	ab212160
Gentamycin	Solarbio, China	G8170
DMEM	Solarbio, China	31600
ELISA Kit for Spp1	EIAab, China	E0899m
ELISA Kit for TGF-β1	Solarbio, China	SEKM-0035
ELISA Kit for Smad2/3	Cell Signaling, USA	12000
ELISA Kit for P-Smad2/3	Cell Signaling, USA	12001
ELISA Kit for Col1a1	Cell Signaling, USA	38499
ELISA Kit for α-SMA	SPBio, China	SP14458
BUN Assay Kit (Urease method)	Nanjing Jiancheng, China	C013-2-1
Creatinine Assay Kit	Nanjing Jiancheng, China	C011-2-1
TGF-β1	Cell Signaling, USA	5231LF

RESOURCE AVAILABILITY

Lead contact

For further information and requests for resources and reagents, please contact [Qi Sun] at [sunqi@njmu.edu.cn].

Materials availability

All unique/stable reagents generated in this study are available from the lead contact with a completed Materials Transfer Agreement.

Data and code availability

The single-cell sequencing dataset GSE139107, pertaining to renal ischemia-reperfusion injury (IRI), was procured from the GEO (Gene Expression Omnibus) repository (http://www.ncbi.nlm.nih.gov/geo/). All data and code supporting the findings of this study are available from the lead contact upon reasonable request.

EXPERIMENTAL MODEL AND STUDY PARTICIPANT DETAILS

Animals

C57BL/6N mice (10–12 weeks old, $Spp1^{+/+}$ wild-type; cs-005, Liaoning Changsheng Biotechnology, Liaoning, China) and Spp1−/− [C57BL/6N-Spp1em1C/Cya, strain number S-KO-04472, Cyagen Biosciences].

Cell lines

Fibroblasts used in the experiments were derived from renal interstitial fibroblasts isolated from C57BL/6N mice. These fibroblasts were self-isolated from mouse kidneys and cultured in DMEM supplemented with 20% fetal bovine serum (FBS), 2 μg/mL fibroblast growth factor (α-FGF), 100 μg/mL gentamycin, 100 IU/mL penicillin, and 100 μg/mL streptomycin. Additionally, 293T cells (CRL-3216, ATCC, USA) were used for lentivirus packaging and were cultured under standard conditions.

METHOD DETAILS

Single-cell RNA sequencing analysis

The single-cell sequencing dataset GSE139107, pertaining to renal ischemia-reperfusion injury (IRI), was procured from the GEO (Gene Expression Omnibus) repository (http://www.ncbi.nlm.nih.gov/geo/). This dataset encompasses data derived from 24 kidney tissue samples obtained from C57BL/6J mice. The sample distribution is as follows: 4 samples in the sham group, 3 samples in the IRI_4 h group (4 h post IRI), 4 samples in the IRI_12 h group (12 h post IRI), 5 samples in the IRI_2d group (2 days post IRI), 4 samples in the IRI_14d group (14 days post IRI), and 4 samples in the IRI_6w group (6 weeks post IRI).

To effectively reduce the dimensionality of the scRNA-Seq dataset, we applied principal component analysis (PCA) utilizing the top 2000 highly variable genes, selected based on their variance. Subsequently, we conducted downstream analysis by identifying the top 20 principal components, determined via the Elbowplot function within the Seurat package. Major cell subpopulations were discerned using the FindClusters function provided by Seurat, with the default resolution parameter set to 0.5. We further harnessed the t-SNE algorithm for nonlinear dimension reduction of the scRNA-seq data. Marker genes characteristic of distinct cell subpopulations were identified through the Seurat package. To enhance cell annotation, we leveraged known cell lineage-specific marker genes and the CellMarker online platform.[49]

Characterization and evolutionary dynamics of fibroblast subpopulations

Eight-week-old healthy C57BL/6N mice were euthanized through cervical dislocation. Subsequently, the kidneys were swiftly excised under aseptic conditions and rinsed with 1×PBS (lacking Ca^{2+} and Mg^{2+}), which included 200,000 IU/L penicillin (YZ-130437, Solarbio, Beijing, China) and 200 mg/L streptomycin (SS8800, Solarbio, Beijing, China). The renal capsule was carefully removed, and the renal cortex was sliced into thin strips measuring 2–3 mm in thickness. These strips were gently ground on a 100-mesh stainless steel wire mesh and rinsed with PBS to gather the filtrate. The filtrate underwent further filtration using a 150-mesh sieve, focusing on collecting interstitial fragments rich in renal tubules. Examination of the collected stromal fragments under an inverted microscope was conducted. If any glomeruli were detected within the collected fragments, additional washing on a 150-mesh sieve was performed until the purity of the renal tubules reached 98% or higher. The suspended renal tubule segments were subsequently placed into culture vials coated with 0.1% gelatin and incubated in a 37°C, 5% CO_2 incubator. The culture medium was refreshed every 4–5 days. Once the cells had proliferated to cover the surface of the vial, they were passaged by trypsin digestion. Passaging was typically carried out every 4–5 days, and generally, by the third generation, relatively pure fibroblasts could be obtained.[31]

Differential gene expression analysis in IRI mouse model

In this study, a total of 7 mice underwent sham surgery, while another 7 mice underwent IRI surgery. On the second day following the surgeries, the mice were anesthetized and humanely euthanized, and both of their kidneys were harvested. To extract RNA from these kidney samples, we utilized Trizol reagent (16096020, Thermo, USA).

The RNA samples were then subjected to assessments to determine their concentration, purity, and integrity. Specifically, we employed the Qubit RNA Analysis Kit (HKR2106-01, Shanghai Bioji Biotechnology Co., Ltd., Shanghai, China) along with the Qubit 2.0 Fluorometer (Q33216, Life Technologies, USA), the Nanometer Spectrophotometer (IMPLEN, USA), and the RNA Nano 6000 Analysis Kit (5067-1511, Agilent, USA) in conjunction with the Bioanalyzer 2100 system. Each sample contained a total of 3 μg of RNA, serving as the input material for RNA sample preparation.

To generate cDNA libraries, we followed the manufacturer's recommendations and employed the NEBNext UltraTM RNA Library Preparation Kit (E7435L, NEB, Beijing, China), which is compatible with Illumina (USA) sequencing technology. Subsequently, the quality of these cDNA libraries was assessed using the Agilent Bioanalyzer 2100 system.

Following the manufacturer's guidelines, we performed clustering of index-encoded samples using the TruSeq PE Cluster Kit v3 cBot HS (Illumina) (PE-401-3001, Illumina, USA) on the cBot cluster generation system. Subsequently, after cluster generation, library preparation was subjected to paired-end sequencing with read lengths of 125 bp/150 bp on the Illumina HiSeq 550 platform.[50,51]

To assess the quality of paired-end reads in the raw sequencing data, we utilized FastQC software v0.11.8. Subsequently, the raw data underwent preprocessing with Cutadapt software version 1.18, which involved the removal of Illumina sequencing adapters and poly(A) tail sequences. Additionally, we eliminated reads with an N content exceeding 5% using a Perl script.

Following these initial steps, we selected sequences with a base quality score of at least 20, which accounted for 70% of the total bases. These high-quality, filtered paired-end sequences were then aligned to the human reference genome using hisat2 software (version 0.7.12).

In the next phase of the analysis, the R language limma package was employed to identify differentially expressed genes (DEGs) using criteria of $|logFC| > 2$ and $p < 0.05$ as the threshold. Heat maps were generated using the Xiantao Academic Online Analysis Tool. Furthermore, gene ontology (GO) and KEGG pathway enrichment analyses of the DEGs were performed utilizing Xiantao Scholar, Metascape, and other relevant tools.[52,53]

Lasso regression analysis is a mathematical modeling technique aimed at elucidating the connection between a dependent variable and one or more independent variables. It involves constructing a quantitative equation that represents this relationship. To build such a model, we can employ the 'glmnet()' function package within the R Studio software. This package enables the loading of a candidate gene matrix and facilitates the selection of an appropriate λ value. For internal validation and the identification of the optimal model, a 10-fold cross-validation approach is applied, especially when α is set to 1.[54]

ElasticNet regression is a statistical analysis technique that combines elements from both Lasso and Ridge regression methods. It is particularly effective in addressing issues related to feature selection and multicollinearity. During the implementation of ElasticNet regression, two crucial parameters are configured using the 'glmnet()' function. These parameters are λ, which represents the regularization parameter responsible for controlling model complexity and preventing overfitting, and α, which serves as the mixing parameter, determining the balance between Lasso and Ridge regularization techniques. The optimal values for λ and α are determined through the use of cross-validation techniques.[54]

ROC curves based on candidate gene expression values were generated using the pROC package in the R language, employing both training and validation datasets. These curves served as an assessment of the accuracy of gene expression in determining the disease status of the samples.[55,56]

Immunohistochemical staining and ELISA assays

Following the harvest of mouse renal tissue, it was fixed overnight using 4% paraformaldehyde (BL539A, Biosharp, USA). Subsequently, tissue sections were cut to a thickness of 4 μm, deparaffinized using xylene (YS176723, Solarbio, Beijing, China), and subjected to a gradient alcohol hydration process (3 min each in anhydrous ethanol, 95% ethanol, and 75% ethanol).

The samples were then immersed in a 0.01 M citrate buffer (SC9350, Solarbio, Beijing, China) and boiled for 15-20 min to facilitate antigen retrieval. Afterward, they were left to incubate at room temperature for 30 min, and 3% H2O2 was employed to deactivate endogenous peroxidase. Following this step, a goat serum-blocking solution was added, allowed to sit at room temperature for 20 min, and excess liquid was removed. The primary antibodies Spp1 (K200110M, Solarbio, Beijing, China), Col1a1 (PA5-29569, Thermo Fisher, USA), α-SMA (ab5694, Abcam, UK), TGF-β1 (ab215715, Abcam, UK), P-Smad2/3 (AF3367, aff biotech, Jiangsu, China), and Smad2/3 (AF6367, aff biotech, Jiangsu, China) were applied at a dilution ratio of 1:200.

Following the 1-h incubation at room temperature, the sample was washed with PBS. Subsequently, the secondary antibody IgG (ab6702, Abcam, USA) was applied at a dilution ratio of 1:500 and incubated at 37°C for 20 min. After another PBS wash, SP drops (Streptavidin-peroxidase) were added, and the sample was incubated at 37°C for 30 min. Following another PBS wash, DAB (P0202, Beyotime, Shanghai, China) was utilized for coloration for 5–10 min, and a 10-min water wash was performed to halt the reaction. The slides were then counterstained with hematoxylin (C0107, Beyotime, Shanghai, China) for 2 min. Subsequently, they were subjected to differentiation in hydrochloric acid alcohol, rinsed with water for 10 min, and dehydrated with a graded alcohol series using xylene as a clearing agent. Finally, 2–3 drops of neutral resin sealant were added. Using an upright microscope, the following results were observed and recorded: 5 high-power fields of view were randomly selected from each slide, 100 cells were counted in each field of view, and the positivity rate of the cells was recorded.[57]

Total protein was extracted from mouse renal tissues, and ELISA kits were employed to assess the protein levels of various molecules including Spp1 (E0899m, EIAab, Wuhan, China), TGF-β1 (SEKM-0035, Solarbio, Beijing, China), Smad2/3 (12000, cell signal, USA), P-Smad2/3 (12001, cell signal, USA), Col1a1 (38499, cell signal, USA), and α-SMA (SP14458, spbio, Wuhan, China) in these renal tissues.[57]

Isolation and cultivation of renal interstitial fibroblasts

Eight-week-old healthy C57BL/6N mice were euthanized through cervical dislocation. Subsequently, the kidneys were swiftly excised under aseptic conditions and rinsed with 1×PBS (lacking Ca2+ and Mg2+), which included 200,000 IU/L penicillin (YZ-130437, Solarbio, Beijing, China) and 200 mg/L streptomycin (SS8800, Solarbio, Beijing, China). The renal capsule was carefully removed, and the renal cortex was sliced into thin strips measuring 2–3 mm in thickness. These strips were gently ground on a 100-mesh stainless steel wire mesh and rinsed with PBS to

gather the filtrate. The filtrate underwent further filtration using a 150-mesh sieve, focusing on collecting interstitial fragments rich in renal tubules. Examination of the collected stromal fragments under an inverted microscope was conducted. If any glomeruli were detected within the collected fragments, additional washing on a 150-mesh sieve was performed until the purity of the renal tubules reached 98% or higher. The suspended renal tubule segments were subsequently placed into culture vials coated with 0.1% gelatin and incubated in a 37°C, 5% CO2 incubator. The culture medium was refreshed every 4–5 days. Once the cells had proliferated to cover the surface of the vial, they were passaged by trypsin digestion. Passaging was typically carried out every 4–5 days, and generally, by the third generation, relatively pure fibroblasts could be obtained.[31]

Cell transfection

Fibroblasts with Spp1 knockdown and Spp1 overexpression were generated through lentivirus transfection, utilizing the knockdown sequence specified in Table 1. Plasmid construction and lentivirus packaging services were provided by TransGen Biotech (Shanghai, China). The plasmids, which carried the firefly luciferase reporter gene and the helper plasmid, were co-transfected into 293T cells (CRL-3216, ATCC, USA). Validation, amplification, and purification steps were performed to obtain the packaged lentivirus. For cell transfection mediated by lentivirus, 5 × 105 cells were seeded in a 6-well plate. When the cell confluency reached 70–90%, an appropriate volume of the packaged lentivirus (MOI = 10, working titer approximately 5 × 106 TU/mL) and 5 μg/mL polybrene (Merck, TR-1003, USA) were added to the culture medium. After 4 h of transfection, an equal volume of culture medium with diluted polybrene was introduced. Following 24 h of transfection, the fresh culture medium replaced the existing medium. After 48 h of transfection, the transfection efficiency was assessed through luciferase reporter gene analysis, and stably transfected cell lines were selected by applying 1 μg/mL puromycin (Thermo Fisher, A1113803, USA) for resistance screening.

The *in vitro* cell validation experiments were divided into the sh-NC group, sh-Spp1 group, oe-NC group, and oe-Spp1 group. The cell experiments were repeated three times.[31]

RT-qPCR, CCK-8, and western blot

To extract total cellular RNA, cell lysis was performed using Trizol reagent (R0011, anytime, Shanghai, China), followed by RNA quality and concentration assessment using a UV-visible spectrophotometer (ND-1000, Nanodrop, USA). For the detection of mRNA expression levels, reverse transcription was carried out using the PrimeScript RT-qPCR Kit (RR014, TaKaRa, USA). Real-time quantitative reverse transcription polymerase chain reaction (RT-qPCR) was conducted with the SYBR Premix Ex TaqTM (RR820, TaKaRa, USA) on the LightCycler 480 system (Roche Diagnostics, Pleasanton, CA, USA). GAPDH served as the internal control for mRNA quantification, ensuring precise relative expression measurements. Please refer to Table 2 for primer sequences. Relative fold changes in target gene expression between the experimental and control groups were determined using the 2-ΔΔCt method, where ΔΔCt equals ΔCt in the experimental group minus ΔCt in the control group. Here, ΔCt represents the Ct value of the target gene minus the Ct value of the reference gene.[31]

Cell viability was assessed following the protocol provided by the CCK-8 assay kit (ab228554, Abcam, USA). Cells from each group were seeded into a 96-well plate, with 2500 cells per well, and cultured for different time intervals: 12, 24, 36, and 48 h. At each specified time point, 10 μL of CCK-8 solution was added to each well. After a 2-h incubation period, the absorbance at a wavelength of 450 nm was measured using an enzyme-linked immunosorbent assay (ELISA) reader, specifically the Tecan M1000 PRO reader.[58]

The cultured cells were first digested and collected using trypsin, and then cell lysis buffer (P0013, Beyotime, Shanghai, China) was employed to lyse the cells. The protein concentration was determined using the BCA protein quantification kit (P0010, Beyotime, Shanghai, China).

Next, SDS-PAGE was used to separate the proteins, which were subsequently transferred onto a PVDF membrane. The membrane was blocked with 5% BSA at room temperature for 1 h. Primary antibodies, including Spp1 (K002763P, solarbio, Beijing, China), Colla1 (PA5-29569, Thermo Fisher, USA), GAPDH (ab8245, Abcam, UK), α-SMA (ab5694, Abcam, UK), P-Smad2/3 (8828, Cell Signaling Technology, USA), and Smad2/3 (8685, Cell Signaling Technology, USA), were diluted and added separately. This was followed by overnight incubation at 4°C. The membrane was then washed three times with PBST (each wash lasting 5 min) and subsequently incubated at room temperature with a goat anti-rabbit secondary antibody (Catalog number A0277, anytime, Shanghai, China) for 1 h. After three additional PBST washes (each lasting 5 min), excess PBST was removed, and an appropriate amount of ECL working solution (P0018S, anytime, Shanghai, China) was added. The transfer membrane was then incubated at room temperature for 1 min. Excess ECL reagent was removed, the membrane was sealed with plastic wrap, and it was placed in a dark box for 5–10 min of X-ray film exposure, followed by development and fixing. The quantification of bands in Western blot images from different groups was performed using ImageJ analysis software, with GAPDH serving as the internal ref. [59,60].

Wound healing and transwell assays

To prepare single-cell suspensions for each cell group exhibiting robust growth, the aforementioned method was employed. The cell count was determined for each group, and the cell suspension was then inoculated into a six-well plate containing 2 mL of culture medium, with a cell density of 8×10^5 cells/mL. These plates were subsequently placed in a 37°C incubator with 5% CO_2, and cells were cultured until reaching a cell density of 90%–100%. Using a 200 μL pipette tip, a vertical "—"-shaped scratch was gently created along the surface of the plate. Afterward, the plate was washed twice with PBS to eliminate any suspended cells, and serum-free RPMI 1640 medium was added. The cells were

further incubated for 24 h, and images were captured to calculate the scratch healing rate. The formula used to determine the scratch healing rate is as follows: (initial scratch width - final scratch width)/initial scratch width × 100%.[61] This experiment was repeated three times.

A transwell culture chamber with an 8 μm pore size (SBM07797, Solelybio, Beijing, China) was utilized to assess the impact of Spp1 on cell migratory capability. Initially, fibroblast cells from the P3 passage were resuspended at a concentration of 5 × 104 cells per well, and 200 μL of this cell suspension was seeded into the upper chamber of the Transwell. Subsequently, the Transwell system was incubated at 37°C in a CO_2 incubator for a duration of 24 h. Following the incubation period, the culture medium in the lower chamber of the Transwell was aspirated, the chamber was washed twice with PBS buffer, and the cells were fixed with 4% polyformaldehyde (PFA) at room temperature for 30 min. After fixation, any remaining fibroblasts on the upper surface of the Transwell were gently removed using a cotton swab. Subsequently, the Transwell was immersed in a 0.1% crystal violet staining solution (G1063, Solarbio) for 20 min in the lower chamber. Finally, the stained fibroblast cells were examined under an optical microscope.[62,63]

Immunofluorescent staining

The slides containing cells underwent fixation in 4% PFA (G2130, Solarbio, Beijing, China) for a duration of 30 min. Subsequently, they were subjected to permeabilization and blocking using a combination of 0.3% Triton X-100 (T8200, Solarbio, Beijing, China) and 5% BSA (SA8130, Solarbio, Beijing, China) for 1 h.

For single staining antibody methods, primary antibodies, namely Col1a1 (K002759P, Solarbio, Beijing, China) and α-SMA (YT680, Beyotime, Beijing, China), were diluted at a ratio of 1:300. The slides with cells were incubated in a diluted primary antibody solution at 4°C overnight. Afterward, they were washed three times with PBS and subsequently incubated with Alexa Fluor 647 goat anti-rabbit antibody (catalog number: K0034G-AF647, Solarbio, Beijing, China) at room temperature for 1 h. The dilution ratio for the secondary antibody was 1:500. For double staining antibody methods, the primary antibody for P-Smad2/3 (host: rat, reactivity: mouse) was custom-made by Abcam (Beijing, China) and was also diluted at a ratio of 1:500. The antibodies were diluted according to the recommended dilution ratios and then mixed with another primary antibody in a 1:1 volume ratio. The slides with cells were incubated in a diluted primary antibody solution at 4°C overnight. After washing three times with PBS, a mixture of Alexa Fluor 647 goat anti-rabbit antibody (K0034G-AF647, Solarbio, Beijing, China) and FITC-labeled goat anti-rat antibody (GTCX73, GeneTex, USA) in a 1:1 volume ratio was applied. The mixed secondary antibodies were incubated for 1 h. The dilution ratio for the secondary antibodies was 1:500. Finally, the slides or tissue sections were washed three times with PBS. Positive cell counting for markers in each field of view was conducted using confocal laser scanning microscopy (880, Carl Zeiss AG, Germany). Five random fields were evaluated in each group of each slide or tissue section. Statistical analysis of fluorescence intensity was performed using ImageJ (V1.8.0) software.[64]

TGF-β1 treatments

Fibroblasts were cultured for 48 h in serum-free conditions, a state of cellular starvation. Subsequently, a solution of TGF-β1 (10 ng/mL) (5231LF, cellsignal, UK) was added to the starved cells, and the culture was continued for an additional 24 h. Afterward, cell samples were collected from the culture dish, and the expression levels of myofibroblast markers (Col1a1 and α-SMA) were analyzed using Western blot and immunofluorescence techniques.[30] When employing A83-01 (A3133, Apex Bio, USA) to treat fibroblasts, the dosage used was 1 μM, and the treatment duration lasted for 1 h

QUANTIFICATION AND STATISTICAL ANALYSIS

Single-cell data quantification

Obtained the single-cell RNA sequencing (scRNA-seq) dataset GSE139107 related to acute kidney injury caused by ischemia-reperfusion injury (IRI) from the Gene Expression Omnibus (GEO) database, including 24 kidney tissue samples from mice. Analyzed the data using the Seurat package in R. Initial quality control involved examining the number of genes (nFeature_RNA), the number of mRNA molecules (nCount_RNA), and the percentage of mitochondrial genes (percent.mt) in all cells of the scRNA-seq data. Excluded low-quality cells based on the criteria of nFeature_RNA >300, 300 < nCount_RNA <5000, and percent.mt < 3%. Normalized the experimental data using the "LogNormalize" function, selecting the top 2000 highly variable genes based on gene expression variance for downstream analysis. Performed principal component analysis (PCA) on the 2000 genes for dimensionality reduction, enabling subsequent TSNE clustering of the cells. Selected the top 20 principal components (PCs) for TSNE clustering and cell annotation.

Statistical analysis in experimental studies

Statistical analysis was conducted using SPSS software (version 21.0, IBM, USA). Measurement data are presented as mean values with corresponding standard deviations. To compare two groups, a non-paired t-test was employed, while a one-way analysis of variance (ANOVA) was utilized for comparisons involving multiple groups. Statistical significance was determined at the conventional threshold of $p < 0.05$.[46]